



# Effects of Grain Growth on Molecular Abundances in Young Stellar Objects

Nanase Harada<sup>1</sup>, Yasuhiro Hasegawa<sup>2</sup>, Yuri Aikawa<sup>3</sup>, Hiroyuki Hirashita<sup>1</sup>, Haoyu Baobab Liu<sup>4</sup>, and Naomi Hirano<sup>1</sup>

<sup>1</sup>Institute of Astronomy and Astrophysics, Academia Sinica, P.O. Box 23-141, Taipei 10617, Taiwan; [harada@asiaa.sinica.edu.tw](mailto:harada@asiaa.sinica.edu.tw)

<sup>2</sup>Jet Propulsion Laboratory, California Institute of Technology, Pasadena, CA 91109, USA

<sup>3</sup>Center for Computer Sciences, University of Tsukuba, Tsukuba 305-8577, Japan

<sup>4</sup>European Southern Observatory (ESO), Karl-Schwarzschild-Str. 2, D-85748 Garching, Germany

Received 2016 November 17; revised 2017 February 2; accepted 2017 February 9; published 2017 March 6

## Abstract

Recent observations suggested that the growth of dust grains may have already occurred in class 0/I young stellar objects (YSOs). Since chemical reactions on dust grain surfaces are important in determining molecular abundances, the dust size growth may affect chemical compositions in YSOs significantly. In this work, we aim to determine how grain growth affects chemical abundances. We use a time-dependent gas-grain chemical model for a star-forming core to calculate the gas-phase and grain-surface chemical abundances with variation of surface areas of grains to imitate grain growth. We also perform parameter studies in which the initial molecular abundances vary. Our results show that a smaller extent of the surface areas caused by grain growth changes the dominant form of sulfur-bearing molecules by decreasing H<sub>2</sub>S abundances and increasing SO and/or SO<sub>2</sub> abundances. We also find that complex organic molecules such as CH<sub>3</sub>CN decrease in abundances with larger grain sizes, while the abundance of other species such as CH<sub>3</sub>OCH<sub>3</sub> is dependent on other parameters such as the initial conditions. Comparisons with observations of a class 0 protostar, IRAS 16293-2422, indicate that the observed abundance ratios between sulfur-bearing molecules H<sub>2</sub>S, SO, and SO<sub>2</sub> can be reproduced very well when dust grains grow to a maximum grain size of  $a_{\max} = 10\text{--}100\ \mu\text{m}$ .

*Key words:* astrochemistry – dust, extinction – ISM: molecules – stars: protostars

## 1. Introduction

The formation of stars and planets is intimately linked (e.g., Li et al. 2014 for a recent review). For example, planet formation is a natural outcome of star formation, possibly via circumstellar disks (e.g., Benz et al. 2014). Dust growth is a crucial process that can affect star and planet formation (e.g., Natta et al. 2007). This is partly because the presence of (small) dust particles regulates the degree of coupling between magnetic fields and star-forming materials (e.g., Zhao et al. 2016). As a result, when dust growth proceeds in star-forming clouds, which can reduce the number density of small dust particles, the dynamics of these clouds can be affected significantly. For planet formation, dust growth serves as one of the first steps of forming building blocks of planets (e.g., Testi et al. 2014). Furthermore, it has recently received a huge attention that accretion of pebble-sized dusty particles can speed up the formation of planetary cores significantly (e.g., Johansen et al. 2015). As a result, it is of fundamental importance to understand how dust growth proceeds in star-forming environments in order to fully examine how star and planet formation takes place simultaneously.

Radio interferometric observations have suggested that such millimeter-sized grains would be needed to fully reproduce the millimeter opacity spectral index (the so-called  $\beta$  index) obtained for class 0–I young stellar objects (YSOs, e.g., Jørgensen et al. 2007; Kwon et al. 2009; Ricci et al. 2010; Chiang et al. 2012; Tobin et al. 2013; Miotello et al. 2014). In general, the value of  $\beta$  is derived from multiwavelength observations and is used as a probe to investigate whether millimeter-sized grains are present in the systems. Fitting of observational results indicates that dust grains of 1 mm or larger are necessary to explain the opacity index of

$\beta \lesssim 1$  between  $\lambda = 1$  and 3 mm (Ricci et al. 2010; Kataoka et al. 2014).<sup>5</sup>

While observations to derive  $\beta$  in class 0–I YSOs are mostly done by single-dish telescopes, which do not fully resolve the source, some class 0 protostars exhibit a low value of  $\beta (< 1)$  even in their envelopes (Kwon et al. 2009; Chiang et al. 2012; Miotello et al. 2014). These observational results suggest that millimeter-sized grains can exist not only in the vicinity of protostars ( $\lesssim 100$  au), but also on larger scales ( $\sim 1000$  au) of protostellar envelopes. Furthermore, this trend of low  $\beta (\lesssim 1)$  is reported for YSOs located in a number of star-forming regions such as Perseus (e.g., Jørgensen et al. 2007; Kwon et al. 2009), Taurus (e.g., Jørgensen et al. 2007), Cepheus (e.g., Kwon et al. 2009), and  $\rho$ -Oph (Ricci et al. 2010). Consequently, the presence of larger ( $\sim 1$  mm) dust grains may be a common property in class 0–I YSOs, while the origin of such grains is still poorly known.

On the other hand, it is currently recognized theoretically that dust growth is not efficient enough to form millimeter-sized grains in star-forming regions. This recognition was made by theoretical studies (e.g., Ormel et al. 2009; Hirashita & Li 2013), based on the properties of star-forming clouds: their volume densities are very low, and their lifetimes are too short ( $\lesssim 10^4$  year) for dust particles to coagulate efficiently via collisions. Instead, physical conditions in the vicinity of the protostar ( $R \sim 10$  au) with high enough density ( $n \sim 10^{10}\ \text{cm}^{-3}$ ) are needed for large grains to form (Wong et al. 2016). This implies that the presence of large ( $\sim 1$  mm) dust grains would be very rare in star-forming clouds theoretically. This inconsistency between theoretical and

<sup>5</sup> Note that in addition to a possible presence of large dust grains, other interpretations would also be possible for some of these observations (e.g., see Li et al. 2017).

observational studies makes it useful to have another method to study the degree of grain growth.

Observations of molecular abundance ratios have the potential of providing independent constraints on the properties of protostars and their circumstellar materials (e.g., Herbst & van Dishoeck 2009). This is because some chemical reactions and the resulting molecules directly reflect the background density and temperature. Accordingly, chemical compositions change as molecular clouds evolve from diffuse or translucent clouds to prestellar cores and down to protostars. We can therefore make use of chemistry to probe various stages of star and planet formation. It is interesting that chemical compositions vary among protostars. For instance, the class 0 protostar IRAS 16293-2422 is well known as a typical hot corino that is rich in complex organic molecules (COMs; e.g., Jørgensen et al. 2016). Other famous examples of hot corinos are IRAS 2A and IRAS 4A, which reside in the star-forming region NGC 1333. In contrast, the protostars L1527 and IRAS 15398-3359 are deficient in COMs, but they show emission lines from various carbon-chain molecules. One of the causes that might generate this difference may be the physical environment in which the YSOs were born (e.g., Sakai & Yamamoto 2013).

A number of theoretical studies on chemical compositions in class 0–I YSOs have been carried out so far to investigate physical and chemical processes of star and planet formation (e.g., Dutrey et al. 2014; van Dishoeck et al. 2014 for reviews). These include a modeling of the molecular abundances and line intensities for IRAS 16293 (Doty et al. 2004), and an investigation of how COMs form in star-forming clouds (Aikawa et al. 2008, A08, hereafter). As described above, large grains may already be present in class 0–I YSOs. While the effects of grain growth on chemistry have been explored in cold dense clouds (Acharyya et al. 2011; Pauly & Garrod 2016) and in circumstellar disks around T Tauri stars, also known as protoplanetary disks (e.g., Aikawa & Nomura 2006), the corresponding work has not been undertaken for class 0–I YSOs yet.

In this paper, we incorporate the effects of grain growth into a chemical model and investigate how molecular evolution will be affected by the presence of larger grains in star-forming clouds. In our model, grain growth means grain coagulation and does not indicate accretion of gas-phase materials. Coagulation potentially has a dramatic impact on the total surface area of grains. This becomes possible because the total grain surface area can be scaled with the maximum grain radius ( $a$ ) as  $\propto a^{-0.5}$  if we assume the grain size distribution as  $dn(a)/da \propto a^{-3.5}$  (see Section 2.4). Since the presence of dust grains can act as “catalysts” for some species that can be produced on the dust surface, the abundance of certain molecules would vary significantly as a function of the degree of grain growth. Since these species can be observable when the surrounding temperature becomes high enough for them to sublime, our model may provide a diagnostic tool for the degree of grain growth. This can eventually be translated into a better picture of class 0–I YSOs and of how star and planet formation occurs concurrently.

This paper is organized as follows. The physical and chemical models we use are described in Section 2. We present the results in Section 3, in which we vary the degree of grain growth. In Section 4 we perform a parameter study and examine how the results can be affected by changing the model parameters. In addition, comparisons with observations are

undertaken, and other related issues are also discussed. Finally, Section 5 gives the summary of this paper.

## 2. Physical and Chemical Models

We describe a physical and chemical model that serves as a basis to explore the effect of grain growth on chemical abundance in class 0/I YSOs. Using the initial conditions described in Section 2.3, our calculation of molecular abundances starts from the quiescent phase (Section 2.5), adopting the constant physical condition that is used as the initial condition for the collapse phase (Section 2.1). Then, we run the collapse phase with variable physical conditions described in Section 2.1.

### 2.1. Physical Model

Star formation is the assembly of physical processes, wherein dense starless (prestellar) cores collapse gravitationally to form protostars (e.g., Li et al. 2014 for a recent review). Molecular evolution in star-forming regions is intimately coupled with such dynamical processes (e.g., van Dishoeck & Blake 1998; Aikawa 2013, for a review).

For the physical conditions of a star-forming cloud, we use the same condition as was adopted in A08. They used results from 1D radiation-hydrodynamic calculations to investigate the time evolution of a star-forming cloud (see Masunaga & Inutsuka 2000, for a detailed method). Based on Masunaga & Inutsuka (2000), the physical conditions of densities, temperatures, and visual extinctions of the clouds are obtained, which are used for a chemical evolution model. As done in A08, we adopt the Lagrangian approach to implement a chemical network code into a time-evolving cloud in a post-processing fashion. We thus focus on certain collapsing shells and track them down in time, in order to specify how their physical conditions change as star formation proceeds.

Figure 1 shows the time evolution of the density and the temperature plotted as a function of time  $t$ . We note that the  $x$ -axis is labeled as  $t_{\text{final}} - t$  in order to clearly visualize the later stage of star formation. The final time of our model ( $t_{\text{final}}$ ) is set as  $9.3 \times 10^4$  years. More specifically, we define that  $t = 0$  when a protostar (second core) forms, which is about  $2.5 \times 10^5$  years after the onset of collapse, and the subsequent evolution is followed over  $9.3 \times 10^4$  years. This means that our simulations start at negative times. The plot mainly covers the protostellar stage ( $t_{\text{final}} - t < 10^5$  years). In Figure 1 we pick up layers that are initially located at  $r \sim 10^4$  au and eventually arrive at  $r_{\text{final}} = 2.5, 15, 125,$  and  $1000$  au at  $t_{\text{final}}$ . We provide a brief summary here and refer to A08 for a complete discussion (see Section 3.2 in A08).

Figure 1 (top) shows the corresponding results of the gas density. The density increases monotonically before protostar formation ( $t_{\text{final}} - t \gtrsim 10^5$  years). After this, its increment becomes more rapid, since the collapse timescale decreases with increasing density. In the early stage of collapse, cooling is so efficient that the temperature remains low ( $\sim 7$ – $8$  K) (Figure 1, bottom). As the collapse proceeds, the gravitational heating overwhelms the cooling, and a protostar is eventually formed around  $t_{\text{final}} - t \simeq 10^5$  years, which causes a sudden temperature rise in the infalling envelope. After a protostar is born, the temperature continues to increase.

The values of visual extinction  $A_V$  during the cloud-collapse phase can be calculated from this density distribution using the

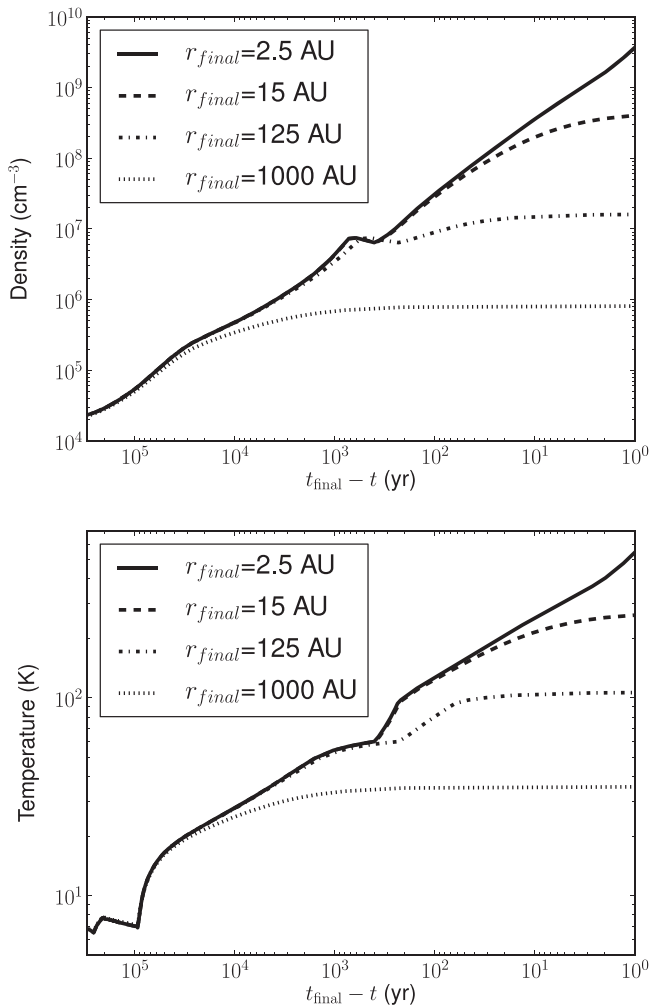


**Figure 1.** The density and the temperature of the protostar model by A08 for  $r_{\text{final}} = 2.5, 15, 125,$  and  $1000$  au.

formula to convert the column density into the visual extinction:  $A_V = N_{\text{H}} / (1.59 \times 10^{21} \text{ cm}^{-2})$ . As in A08, we assume that the core is embedded in the surrounding cloud, and hence 3 mag is added to the computed values of  $A_V$ . In reality, the value of  $A_V$  should change with dust growth because the conversion factor between the column density and the visual extinction is dependent on the dust properties. In this paper, nonetheless, we keep the above-mentioned  $A_V$ - $N_{\text{H}}$  conversion factor in most of our calculations even with the grain growth. This is because, as a first step, we attempt to explore the pure effect of the decrement of the grain surface area on the resulting molecular abundances. This enables a more direct comparison of chemical evolution in class 0/I YSOs between the models with and without grain growth. Furthermore, we find that if the value of  $A_V$  is self-consistently calculated according to a large degree of grain growth,  $A_V$  decreases by orders of magnitude compared with values measured in Bok globules, which is probably unrealistic. We thus consider that usage of the above conversion factor would be suitable for our calculations in this paper. For the completeness, calculations with self-consistently computed  $A_V$  and  $f_{\text{g}}$  are carried out in Section 4.2, however, in order to examine how the reduction of  $A_V$  caused by grain growth affects the molecular abundances.

In the chemistry calculations, we adopt the above physical model under the assumption that both the gas and dust grains have the same temperature, which is plotted in Figure 1. In addition to the temperature coupling of the gas and the dust, the dust temperature can be affected by the grain size. For grains directly exposed to stars, the dust temperature scales with dust size  $a$  with  $T_{\text{dust}} \propto a^{-1/6}$  (Kruegel 2003; Pauly & Garrod 2016). The gas in a protostellar core can be heated by the compressional heating, and the gas can transfer the heat to the dust. It is unlikely that the dust temperature scales as the above relationship, and the detailed consideration of the dust temperature with various dust sizes is left as future work. The maximum temperature achieved by cosmic-ray heating can also be higher for small-sized grains (Herbst & Cuppen 2006). We also ignore the change in the maximum temperature that is due to cosmic-ray heating because the dependence is small when the grain grows more than  $0.1 \mu\text{m}$ . We use the physical condition of a shell arriving at  $r_{\text{final}} = 15$  au in Sections 3.1 and 3.2, and shells that have different values of  $r_{\text{final}}$  in Section 3.3.

## 2.2. Chemical Model

For calculations of chemical abundances, we adopt the gas-grain time-dependent chemical model, *Nautilus* (see Hersant et al. 2009; Semenov et al. 2010, for a complete discussion). We make use of the updated version in which deuterium species are included, while we focus mainly on non-deuterated species in this paper. This implementation is done by U. Hincelin et al. (2017, in preparation). In this updated network, 1574 species are treated, 1101 of which are gas-phase species and 473 of which are grain-surface species. This network has 122,429 reactions that arise both from gas-phase reactions and from reactions that involve dust grains. Gas-phase reactions are extended from KIDA network (<http://kida.obs.u-bordeaux1.fr>), which is a network for non-deuterated species. The network also includes reactions related to grains such as accretion, surface reactions, and thermal and nonthermal desorption. For the accretion reactions of gas-phase species onto dust grains, we use the sticking coefficient of  $\mathcal{S} = 1$  in the rate of accretion,

$$\frac{dn(i, \text{dust})}{dt} = \pi \mathcal{S} a^2 \langle v_i \rangle n(i, \text{gas}) n_d, \quad (1)$$

where  $n(i, \text{gas})$  and  $n(i, \text{dust})$  are the concentrations of species  $i$  in the gas phase and in ice, respectively,  $a$  is the dust radius,  $\langle v_i \rangle$  is the mean velocity of species  $i$  in the gas, and  $n_d$  is the number density of grains. We only consider the accretion of neutral species and assume that charged species do not accrete onto grains. For nonthermal desorption, photodesorption caused by UV-photons (Öberg et al. 2007), cosmic-ray heating (Hasegawa & Herbst 1993), and reactive desorption (Garrod et al. 2007) are all taken into account. The ratio of diffusion to binding energy is 0.5 in our calculations. In this work, only two phases of gas and grain surface reactions are considered, and the distinction between the grain surface and ice bulk mantle is neglected. For rate equations, modified rates that are given by Caselli et al. (1998) are used in this paper.

## 2.3. Initial Conditions of Molecular Abundances

Our chemistry calculations start when the formation of molecular clouds is completed and the subsequent star

**Table 1**  
Elemental Abundances

Elements	Abundances/H
He	$9.75 \times 10^{-2}$
N	$2.47 \times 10^{-5}$
O	$1.80 \times 10^{-4}$
C	$7.90 \times 10^{-5}$
S	$9.14 \times 10^{-8}$
Si	$9.74 \times 10^{-9}$
Fe	$2.74 \times 10^{-9}$
Na	$2.25 \times 10^{-9}$
Mg	$1.09 \times 10^{-8}$
P	$2.16 \times 10^{-10}$
Cl	$1.00 \times 10^{-9}$

formation is about to occur. In other words, molecular abundances at that time will serve as our initial conditions.

To realistically determine these abundances, we adopt the results of Furuya et al. (2015). In their calculations, it is assumed that molecular clouds are formed in the post-shock region after the collision of diffuse gas clouds. Following the physical condition given by Bergin et al. (2004), they calculate the formation of molecules in the post-shock gas. Elemental abundances are summarized in Table 1, which corresponds to the case of “low-metal” abundances in Furuya et al. (2015). These elemental abundances are taken from Aikawa & Herbst (1999) and for the deuterium fraction from Linsky (2003). While Furuya et al. (2015) consider three phases of gas, grain surface, and grain bulk mantle reactions, our work only considers two phases of gas and grain surface reactions. In order to use their output abundances as our initial conditions, we added the grain mantle abundances to the grain surface abundances. Table 2 summarizes the resulting fractional abundances of major species, which are used as the initial conditions for our chemistry calculations. We note that we use the results of Furuya et al. (2015), which have been obtained when the visual extinction ( $A_V^{\text{init}}$ ) reaches the values of  $A_V^{\text{init}} = 1$  mag and 3 mag. The lower value of  $A_V^{\text{init}}$  corresponds to the case where the accumulation of post-shock gas is still low. For the calculations of Section 4.3.1, we also use a sulfur elemental abundance higher by an order of magnitude ( $9.14 \times 10^{-7}$ ) because it agrees better with the observations of fractional abundances.

#### 2.4. Treatment of Grain Growth

In the reaction rate equations, the accretion rate of gaseous species onto dust grains is proportional to the total surface area of grains (see Equation (1)). Here we describe how the total surface area varies with grain growth.

We use a power-law size distribution that is conventional for dust grains in the ISM (Mathis et al. 1977) in order to take the effect of grain growth into account. For this case, the grain size distribution can be given as  $dn(a)/da = n_0 a^{-3.5}$ , where  $dn(a)$  is the number density of dust grains in a radius range of  $a$ – $a + da$  and  $n_0$  is the normalization constant. When the total dust mass density is given as  $\rho_{\text{dust}}$ , we can specify the value of  $n_0$  based on the following equation assuming  $a_{\text{max}} \gg a_{\text{min}}$ :

$$\rho_{\text{dust}} = \int_{a_{\text{min}}}^{a_{\text{max}}} da \frac{4\pi}{3} \rho_{\text{gr}} a^3 (n_0 a^{-3.5}) \simeq \frac{8\pi}{3} \rho_{\text{gr}} n_0 \sqrt{a_{\text{max}}}, \quad (2)$$

**Table 2**

Initial Fractional Abundances with Respect to Total Hydrogen Abundances for Selected Species

Species	$A_V^{\text{init}} = 1$ mag.	3 mag.
p-H <sub>2</sub>	4.76(−1)	5.00(−1)
o-H <sub>2</sub>	2.37(−2)	2.38(−4)
H	5.19(−4)	5.09(−5)
CO	6.07(−5)	5.18(−6)
CO(ice)	1.19(−5)	4.68(−5)
CH <sub>4</sub> (ice)	2.64(−6)	1.83(−5)
C	2.16(−6)	5.69(−7)
CO <sub>2</sub> (ice)	4.21(−7)	1.33(−6)
C <sup>+</sup>	3.55(−7)	2.64(−9)
H <sub>2</sub> CO(ice)	1.79(−7)	2.21(−6)
C <sub>3</sub> H <sub>4</sub> (ice)	2.23(−8)	3.62(−7)
N	1.50(−5)	3.35(−7)
NH <sub>3</sub> (ice)	8.72(−6)	1.83(−5)
N <sub>2</sub>	4.44(−7)	7.40(−7)
N <sub>2</sub> (ice)	2.58(−8)	1.99(−6)
CN	1.33(−8)	4.35(−8)
H <sub>2</sub> O(ice)	8.39(−5)	1.22(−4)
O	2.24(−5)	2.33(−7)
OH	1.56(−8)	1.09(−8)
Si <sup>+</sup>	8.29(−9)	8.16(−11)
Si	5.15(−10)	3.06(−10)
SiO	2.91(−10)	4.16(−11)
SiH	2.13(−10)	9.04(−11)
SiH <sub>4</sub> (ice)	1.68(−10)	7.48(−9)
SiO(ice)	8.53(−12)	8.12(−10)
S <sup>+</sup>	7.71(−8)	2.96(−9)
S	1.34(−8)	7.04(−8)
CS	6.10(−10)	2.73(−9)
H <sub>2</sub> CS(ice)	1.12(−10)	1.06(−8)
Fe <sup>+</sup>	2.66(−9)	6.77(−10)
Fe	6.79(−11)	2.98(−10)
FeH(ice)	1.39(−11)	1.76(−9)
Na <sup>+</sup>	1.81(−9)	2.18(−10)
Na	4.23(−10)	9.30(−10)
Mg <sup>+</sup>	9.75(−9)	2.45(−10)
Mg	8.78(−10)	3.70(−10)
MgH <sub>2</sub> (ice)	2.75(−10)	1.03(−8)
Cl	6.87(−10)	7.94(−11)
Cl(ice)	3.10(−10)	9.19(−10)
P <sup>+</sup>	1.88(−10)	1.41(−12)
P	2.17(−11)	3.85(−11)

**Note.** Molecules that hold significant fractions of each element are shown. The notation  $a(-b)$  means  $a \times 10^{-b}$ .

where  $\rho_{\text{gr}}$  is the bulk density of dust grains, and  $a_{\text{min}}$  and  $a_{\text{max}}$  are the minimum and the maximum grain radius, respectively. We also assumed that grains are compact and spherical. Accordingly, the total surface area per volume ( $S_{\text{MRN}}$ ) can be computed as

$$S_{\text{MRN}} = \int_{a_{\text{min}}}^{a_{\text{max}}} da 4\pi a^2 \frac{dn(a)}{da} \simeq 3 \frac{\rho_{\text{dust}}}{\rho_{\text{gr}}} (a_{\text{min}} a_{\text{max}})^{-1/2}. \quad (3)$$

This equation suggests that when the maximum grain radius grows from  $a_{\text{max},1}$  to  $a_{\text{max},2}$  and the dust mass density ( $\rho_{\text{dust}}$ ) is conserved, the total surface area is decreased by a factor of  $\sqrt{a_{\text{max},2}/a_{\text{max},1}}$ . We note that we here assumed that  $a_{\text{min}}$  stays the same. We make this assumption because even in circumstellar disks around class II T Tauri stars, there is some evidence of small grains (Dullemond & Dominik 2005;

Birnstiel et al. 2009). It is therefore likely that such small grains also exist in the earlier class 0/I stage. Here, we fix  $a_{\min} = 0.005 \mu\text{m}$  (Mathis et al. 1977).

It is important to point out that our chemistry model adopts a uniform grain radius of  $a_{\text{uni}} = 0.1 \mu\text{m}$  for all the runs. The resulting total surface area ( $S_{\text{uni}}$ ) for this uniform grain radius is given as

$$S_{\text{uni}} = 3 \frac{m_{\text{dust}}}{\rho_{\text{dust}} a_{\text{uni}}}. \quad (4)$$

When we assume that  $a_{\max} \simeq 1 \mu\text{m}$  and  $a_{\min} = 0.005 \mu\text{m}$ , the total surface area per volume in each case becomes similar:

$$S_{\text{MRN}}(a_{\max} = 1 \mu\text{m}) \simeq S_{\text{uni}}. \quad (5)$$

Eventually, we can implement the effect of grain growth into our chemistry calculations by reducing the dust-to-gas mass ratio ( $f_g$ ). This reduction effectively corresponds to the decrement in the total surface area of grains per volume ( $S$ ). More specifically, we rewrite  $f_g$  to include the effect of grain growth as

$$\begin{aligned} f_g &\equiv \frac{\rho_{\text{dust}} S_{\text{uni}}}{\rho_{\text{gas}} S} \\ &= \frac{\rho_{\text{dust}} S_{\text{MRN}}(a_{\max}=1\mu\text{m})}{\rho_{\text{gas}} S_{\text{MRN}}(a_{\max})} \\ &= \frac{\rho_{\text{dust}}}{\rho_{\text{gas}}} \sqrt{\frac{1 \mu\text{m}}{a_{\max}}}, \end{aligned} \quad (6)$$

where  $\rho_{\text{gas}}$  is the gas mass density. In our model, a value of  $f_g = 0.01$  is used for the case of no grain growth. For example,  $f_g = 3 \times 10^{-4}$  means in this paper that the typical grain radius is 1000 times larger (i.e., 1 mm) than the standard one.

### 2.5. Quiescent Phases

While molecular abundances at the end of molecular cloud formation are given by Furuya et al. (2015) (see Section 2.3), it is still unknown when star formation occurs in the cloud. In order to take the possibility into account that core-collapse begins well after cloud formation, we insert a quiescent phase, as done by A08. In the quiescent phase, static dense cloud conditions are adopted, and molecular evolution is only computed for a time interval of  $t_{\text{quie}}$ . More specifically, we assume that the initial hydrostatic core (Bonner–Ebert sphere) is static for  $t_{\text{quie}}$ , and calculate the molecular evolution at each shell. It is also assumed that larger grains are already present at the beginning of the quiescent phase. In other words, we assume that the effect of grain growth on chemistry becomes effective in both the quiescent phase and in the subsequent star formation phase. This assumption is supported by the observational result that some degree of grain growth might have already occurred in a starless core (Forbrich et al. 2015).

### 2.6. Parameters in Our Calculations

There are three free parameters in our calculations, which are summarized in Table 3:  $A_V^{\text{init}}$ ,  $f_g$ , and  $t_{\text{quie}}$ . For  $A_V^{\text{init}}$ , two values are considered to examine the effect of the visual extinction on chemistry (see Section 2.3). For  $f_g$ , we change it from the interstellar value of 0.01 to lower values of  $3 \times 10^{-3}$ ,  $1 \times 10^{-3}$ , and  $3 \times 10^{-4}$  (see Section 2.4). These values can be translated into the maximum grain sizes that are increased

**Table 3**  
List of Parameters

Symbol	Meaning	Value
$A_V^{\text{init}}$	Visual extinction	1 mag, 3 mag
$f_g$	Ratio of dust to gas mass	0.01, $3 \times 10^{-3}$ , $1 \times 10^{-3}$ , $3 \times 10^{-4}$
$t_{\text{quie}}$	Length of the quiescent phase (years)	$10^4$ , $10^6$ , $10^7$

**Table 4**  
List of Our Models

	$f_g$	$A_V^{\text{init}}$	$t_{\text{quie}}$ (year)	$A_V$ Scaling with $f_g$
A1 (Fiducial case)	0.01	3 mag	$10^6$	No
A2 (Grain growth)	$3 \times 10^{-3}$	3 mag	$10^6$	No
A3 (Grain growth)	$10^{-3}$	3 mag	$10^6$	No
A4 (Grain growth)	$3 \times 10^{-4}$	3 mag	$10^6$	No
B1 (Effects of $A_V^{\text{init}}$ )	0.01	1 mag	$10^6$	No
B2 (Effects of $A_V^{\text{init}}$ )	$3 \times 10^{-3}$	1 mag	$10^6$	No
B3 (Effects of $A_V^{\text{init}}$ )	$10^{-3}$	1 mag	$10^6$	No
B4 (Effects of $A_V^{\text{init}}$ )	$3 \times 10^{-4}$	1 mag	$10^6$	No
Ca1 (Effects of $t_{\text{quie}}$ )	0.01	3 mag	$10^4$	No
Ca2 (Effects of $t_{\text{quie}}$ )	$3 \times 10^{-3}$	3 mag	$10^4$	No
Ca3 (Effects of $t_{\text{quie}}$ )	$10^{-3}$	3 mag	$10^4$	No
Ca4 (Effects of $t_{\text{quie}}$ )	$3 \times 10^{-4}$	3 mag	$10^4$	No
Cb1 (Effects of $t_{\text{quie}}$ )	0.01	3 mag	$10^7$	No
Cb2 (Effects of $t_{\text{quie}}$ )	$3 \times 10^{-3}$	3 mag	$10^7$	No
Cb3 (Effects of $t_{\text{quie}}$ )	$10^{-3}$	3 mag	$10^7$	No
Cb4 (Effects of $t_{\text{quie}}$ )	$3 \times 10^{-4}$	3 mag	$10^7$	No
D1 (Effects of scaling $A_V$ )	0.01	3 mag	$10^6$	Yes
D2 (Effects of scaling $A_V$ )	$3 \times 10^{-3}$	3 mag	$10^6$	Yes
D3 (Effects of scaling $A_V$ )	$10^{-3}$	3 mag	$10^6$	Yes
D4 (Effects of scaling $A_V$ )	$3 \times 10^{-4}$	3 mag	$10^6$	Yes

by factors of 10, 100, and 1000, respectively (see Equation (6)). For  $t_{\text{quie}}$ , three values are adopted and take  $10^6$  years as a fiducial value, and we also adopt  $10^4$  years and  $10^7$  years later in Section 4.1.2. We here study the effect of each parameter on molecular evolution (Table 4). In addition, we show results when the values of  $A_V$  are scaled with each value of  $f_g$  as mentioned in Section 2.1. These models are also included in Table 4 as Models D1-4, and they are discussed in Section 4.2.

## 3. Results

We here present our results for the models both with and without grain growth (see Models A1-4 in Table 4). We use the physical condition of a shell that arrives at  $r_{\text{final}} = 15$  au at the final time of our calculation (see Figure 1). Although observations at this scale are challenging even for the Atacama Millimeter/submillimeter Array (ALMA), we choose to show this scale because  $r_{\text{final}} = 15$  au covers chemistry at a wide range of physical conditions. Since the chemistry is more dependent on the physical conditions than the time in our calculation, results of  $r_{\text{final}} = 15$  au at various times also resemble the chemistry at different radii (Section 3.3).

As expected, when the surface areas decrease due to grain growth, accretion of atoms and/or molecules onto dust grains becomes inefficient. This inefficiency causes various changes in the resulting molecular abundances. We examine these changes in detail below.

## Model A1

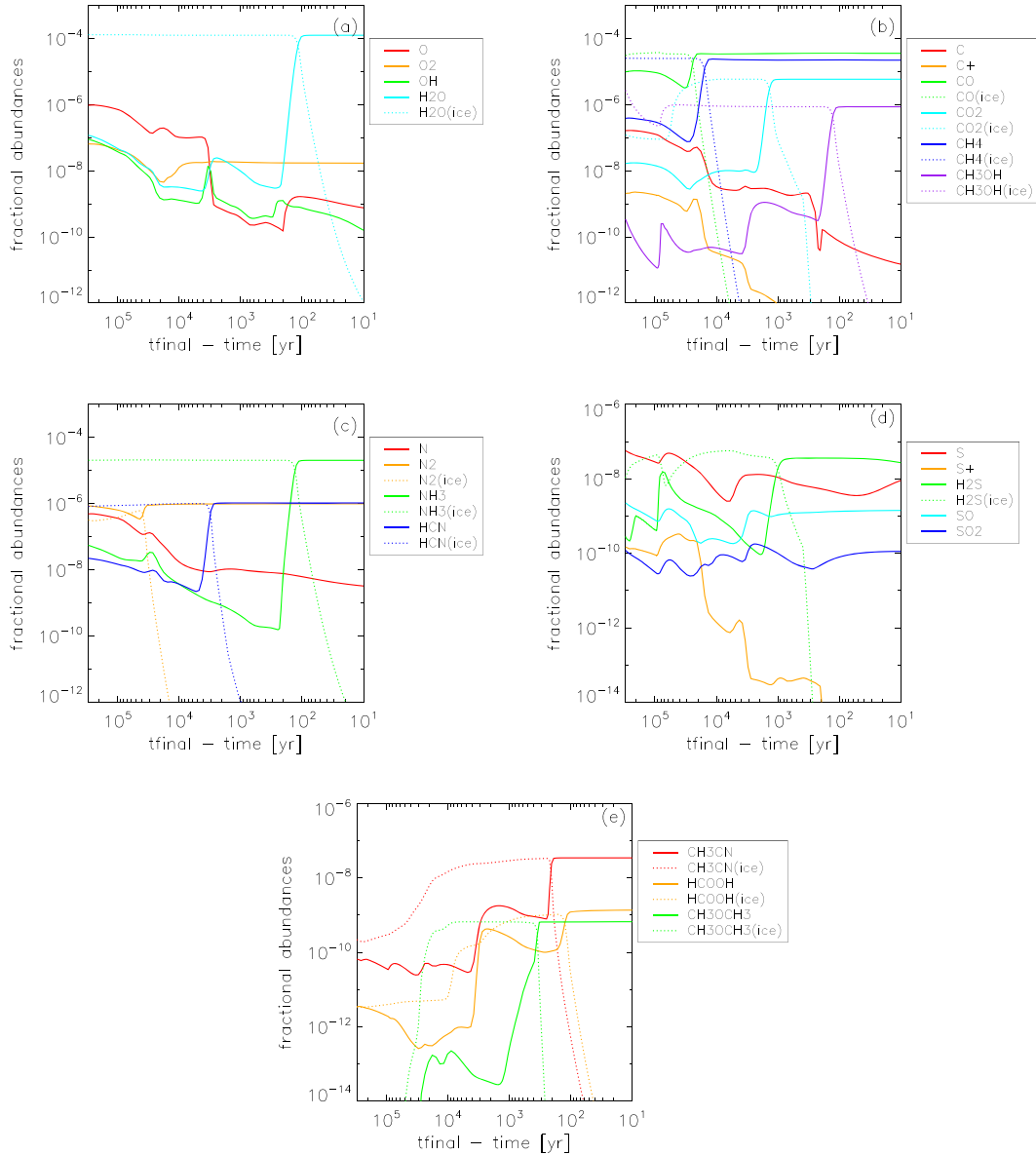


**Figure 2.** Fractional abundances of (a) main oxygen-bearing molecules, (b) main carbon-bearing molecules, (c) main nitrogen-bearing molecules, (d) main sulfur-bearing molecules, and (e) complex organic molecules as a function of  $t_{\text{final}} - t$  for the fiducial case ( $f_g = 0.01$ ,  $t_{\text{quie}} = 10^6$  years, and  $A_{V,\text{init}} = 3$  mag).

### 3.1. The Case of No Grain Growth

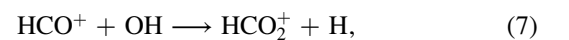
Before we explore the case with grain growth, we first discuss the overall chemistry without grain growth. We compare these results with the results that include grain growth later.

#### 3.1.1. Dominant Forms of O, C, and N

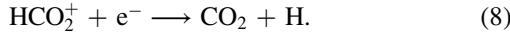
We here start by discussing the overall chemistry of the most abundant species. The dominant forms of oxygen, carbon, and nitrogen are shown in Figure 2. Of the oxygen-bearing molecules, the majority of oxygen is contained in the form of water ice. This is a direct reflection of the initial conditions, which are given by the calculation of Furuya et al. (2015, also see Table 2); in the low-temperature environment, an atomic oxygen on dust can be easily hydrogenated. A

small fraction of oxygen still remains in the form of atomic oxygen, molecular oxygen, OH, CO, and water in the gas phase and the CO ice (Figures 2(a) and (b)). The water ice sublimates into the gas-phase as the temperature reaches  $T \sim 150$  K (Figure 1).

There are several dominant forms of carbon-bearing molecules, CO, CH<sub>4</sub>, CO<sub>2</sub>, and CH<sub>3</sub>OH (Figure 2(b)). While CO has efficient formation reactions in the gas phase (e.g.,  $C + O_2 \rightarrow CO + O$  at the beginning of our calculations), CH<sub>4</sub> can be formed on grain surface by hydrogenation of a carbon atom. As for the case of water ice, the high abundances of these two molecules (CO and CH<sub>4</sub>) are already achieved at the initial conditions (see Table 2). For CO<sub>2</sub> formation, gas-phase reactions are more dominant at the beginning:



followed by



After  $t_{\text{final}} - t \sim 3 \times 10^4$  years,  $\text{CO}_2$  sublimates in the ice phase. The main formation routes of  $\text{CO}_2$  on grains are



or



Methanol ( $\text{CH}_3\text{OH}$ ) is also known to be mainly made on grains via succession of hydrogenation reactions of  $\text{CO}$  ice. This occurs because gas-phase formation routes of methanol are rather inefficient. Our results also indicate different sublimation temperatures for different carbon-bearing molecules. This is clearly shown by examining the times at which grain-surface species turn into gas-phase species. The values of sublimation temperatures are  $\sim 20$  K for  $\text{CO}$  and  $\text{CH}_4$ ,  $\sim 50$  K for  $\text{CO}_2$ , and  $\sim 100$  K for  $\text{CH}_3\text{OH}$ .

Ammonia ( $\text{NH}_3$ ) on the ice is the dominant form of nitrogen, which has already formed by the time of our initial condition (Figure 2(c)). Some amounts of  $\text{N}$  and  $\text{N}_2$  are in the gaseous phase, and  $\text{HCN}$  and  $\text{N}_2$  on ice at the beginning of the run. Following the collapse of a star-forming cloud and the resulting warmup of the cloud,  $\text{HCN}$  sublimates at  $T \sim 50$  K and  $\text{NH}_3$  at  $T \sim 100$  K (see Figure 1).

### 3.1.2. Sulfur-bearing Molecules

Sulfur species are less abundant than C-, N-, and O-bearing molecules because most sulfur is depleted onto grain cores in dense clouds. However, they can act as interesting diagnostics of grain growth, as we discuss in later sections.

The fractional abundances of dominant forms of sulfur are shown in Figure 2(d). From atomic sulfur, which is the most abundant even after chemical evolution in the quiescent phase (see Table 2),  $\text{H}_2\text{S}$  is efficiently made on grains through hydrogenation before  $t_{\text{final}} - t = 10^5$  years. There are moderate fractions of sulfur in  $\text{SO}$  and  $\text{SO}_2$  in the gas-phase, which are formed via the following reactions:



and

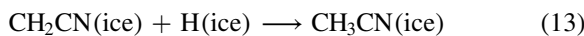


respectively.

### 3.1.3. COMs and Related Molecules

COMs are defined as carbon-bearing molecules with six or more atoms by Herbst & van Dishoeck (2009). They are observed abundantly in prestellar cores and around the protostars. Oxygen-bearing and more hydrogenated or saturated COMs are known to be more abundant around protostars.

We show fractional abundances of such COMs and  $\text{HCOOH}$  (not a COM by definition) in Figure 2(e). Another COM,  $\text{CH}_3\text{OH}$ , has been discussed in Section 3.1.1. Grain surface reactions are essential to form some COMs like methanol mentioned above. Although  $\text{CH}_3\text{CN}$  can be formed in the gas-phase, more efficient formation routes are on grain surfaces via reactions

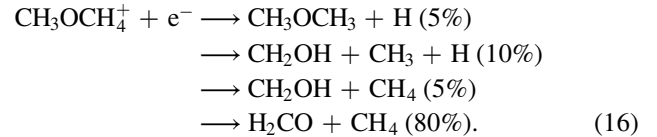
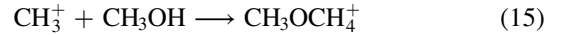


and

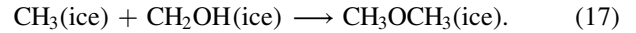


where the progenitor,  $\text{CH}_2\text{CN(ice)}$  is formed via succession of hydrogenation of  $\text{C}_2\text{N}$  on grains.  $\text{C}_2\text{N}$  can be formed in multiple ways such as formation from  $\text{C}$  and  $\text{CN}$  on ice or in the gas-phase via  $\text{N} + \text{C}_2\text{H}$ .

Dimethyl ether ( $\text{CH}_3\text{OCH}_3$ ) can be produced both in the gas phase and on grain surfaces. Before  $t_{\text{final}} - t \sim 5 \times 10^4$  year, the gas-phase formation route is more dominant via succession of reactions, one of whose products is  $\text{CH}_3\text{OCH}_3$ :



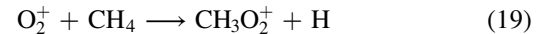
The percentages shown after reaction (16) are the branching ratios. We note that  $\text{CH}_3\text{OCH}_4^+$  is not shown in Figure 2(e). After  $t_{\text{final}} - t \sim 5 \times 10^4$  year, the grain-surface reaction serves as a dominant route, which involves the reaction



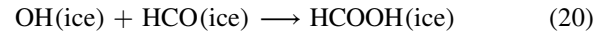
For  $\text{HCOOH}$ , its main formation reactions before it sublimates from ice around  $t_{\text{final}} - t \sim 100$  years are either by



or by a dissociative recombination reaction of  $\text{CH}_3\text{O}_2^+$ , both of which occur in the gas phase. We note that  $\text{CH}_3\text{O}_2^+$  can be made by a reaction



in the gas phase.  $\text{HCOOH}$  in ice is formed by the reaction



on grain surfaces.

## 3.2. Effects of Grain Growth

In this section, we discuss the effects of grain growth by varying  $f_g$  from  $10^{-2}$  to  $3 \times 10^{-3}$ ,  $1 \times 10^{-5}$ , and  $3 \times 10^{-4}$  (see Models A2-4 in Table 4). As in the last section, we focus on the shell with  $r_{\text{final}} = 15$  au. Because the surface area decreases through grain growth, surface reactions on grains and sticking reactions onto grains become less efficient. We may then expect that fractional abundances of molecules that are mainly formed on grain surfaces would decrease as a result of the reduced surface areas. As discussed below, this expectation is valid for some molecules. For other molecules, however, the dependence on grain growth is more complex because the behavior of these molecules is often determined by reaction rates of various formation and destruction processes. We describe the resulting abundance of the molecules below in detail by focusing on the abundant molecules.

### 3.2.1. Dominant Forms of O, C, and N

We find that water ice remains the most abundant form of oxygen (Figure 3, top) even when grain growth is included; the fractional abundances stay almost the same in all the values of  $f_g$ , while the smaller total surface area of dust grains slightly decreases the formation efficiency of water ice there. These

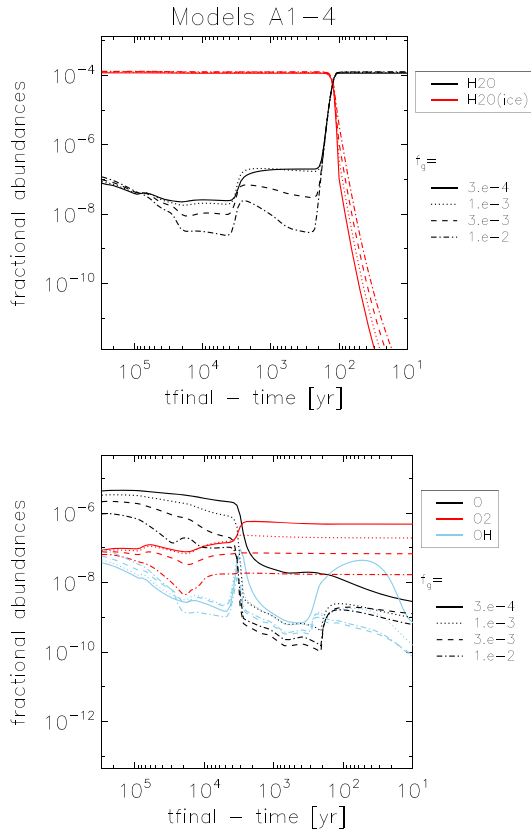


**Figure 3.** Fractional abundances of the main oxygen-bearing molecules as a function of time are shown for an initial condition of  $A_V^{\text{init}} = 3$  mag and  $t_{\text{qui}} = 10^6$  year. Models with different values of  $f_g$  are shown.

slight decreases in water abundances cause significant increases of other oxygen species. For instance, the abundances of atomic and molecular oxygen are increased by about a factor of 10 when the maximum grain size becomes 1000 times larger than in the ISM (Figure 3, bottom). Since OH and O can react to form  $\text{O}_2$ , changes in fractional abundances of OH are not a simple function of the degree of grain growth.

Our results also show that inclusion of grain growth increases the abundance of CO in the gas phase (Figure 4, top). This occurs because sticking of CO onto grains is less efficient. In contrast,  $\text{CH}_4$  decreases in its fractional abundance with grain growth, since it forms predominantly via grain surface hydrogenation (Figure 5, bottom). It is interesting that the abundance of  $\text{CH}_3\text{OH}$  increases with grain growth, which may not be intuitive, considering that the molecules form via grain surface reactions (Figure 5, top). This behavior can be understood as follows: CO on ice can be transformed into either  $\text{CO}_2$  with a reaction with OH or into  $\text{CH}_3\text{OH}$  via successive reactions with atomic hydrogen on ice (through HCO,  $\text{H}_2\text{CO}$ ,  $\text{CH}_2\text{OH}$ , and  $\text{CH}_3\text{OH}$ ). With grain growth, the reaction leading to  $\text{CH}_3\text{OH}$  is favored because a fractional abundance of atomic hydrogen on grains does not decrease with grain growth as much as OH on grains. Thus fractional abundances of  $\text{CH}_3\text{OH}$  become an increasing function of  $1/f_g$ . The abundance of  $\text{CO}_2$  then decreases with grain growth (Figure 4, bottom).

For nitrogen-bearing molecules, the fractional abundances of  $\text{NH}_3$  slightly decrease with grain growth (Figure 6, top). This arises from the fact that grain surface reactions play a dominant role in generating  $\text{NH}_3$  as found for water and  $\text{CH}_4$ . The nitrogen abundances that become available from the decreased

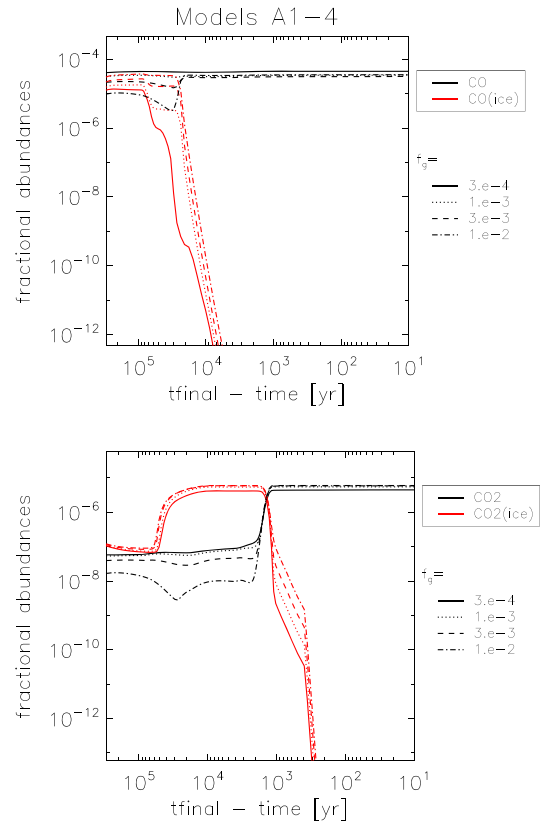


**Figure 4.** Similar to Figure 3, but for some main carbon-bearing molecules.

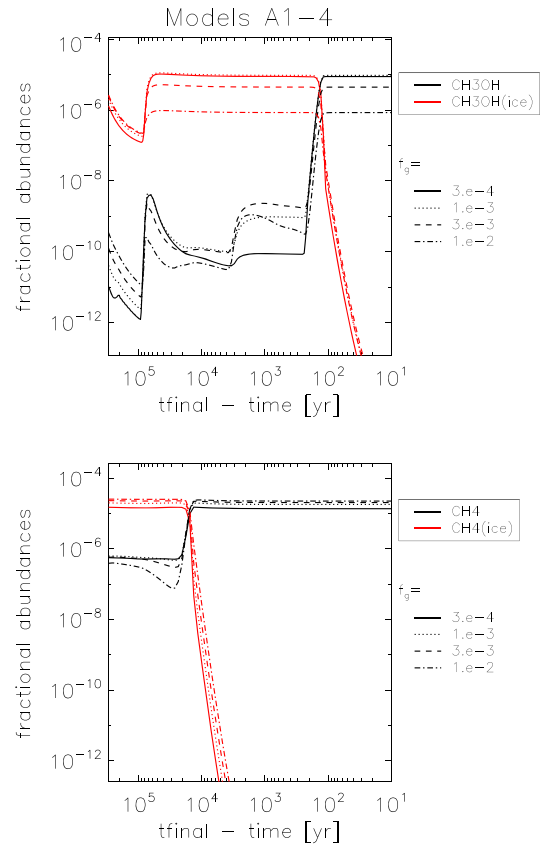


**Figure 5.** Similar to Figure 3, but for additional main carbon-bearing molecules.

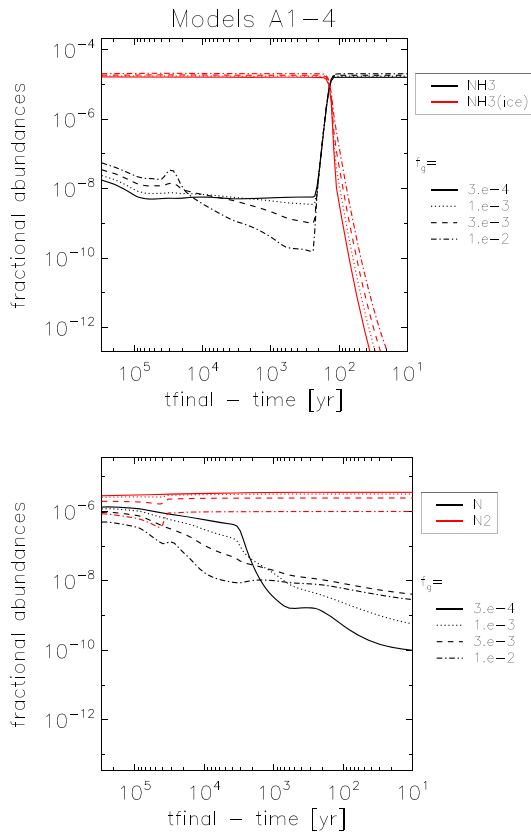


Figure 6. Similar to Figure 3, but for main nitrogen-bearing molecules.

$\text{NH}_3$  lead to slightly increased abundances of molecular  $\text{N}_2$  (Figure 6, bottom). The fractional abundance of  $\text{HCN}$  changes by less than a factor of a few in the grain growth case, and the corresponding results are not shown in this paper.

### 3.2.2. Sulfur-bearing Molecules

We find that sulfur-bearing molecules are the most important in examining the effect of grain growth on molecular evolution. This is because  $\text{H}_2\text{S}$  is made by hydrogenation reactions on grain surfaces. As shown in Figure 7 (top left), lower values of  $f_g$  suppress fractional abundances of  $\text{H}_2\text{S}$  because there is less atomic sulfur on ice. This decrease in  $\text{H}_2\text{S}$  fractional abundance in turn yields other sulfur-bearing molecules ( $\text{SO}$  and  $\text{SO}_2$ ) as the dominant form (Figure 7, top right).

### 3.2.3. COMs and Related Molecules

We now consider the results of COMs and other molecules. As discussed in Section 3.1.3, the main reactions that form  $\text{CH}_3\text{CN}$  occur on grain surfaces either via  $\text{CH}_2\text{CN}$  with  $\text{H}$  (ice) (see Equation (13)), which is more efficient in Model A1, or via  $\text{CH}_3$  with  $\text{CN}$  (ice) (see Equation (14)). Inclusion of grain growth leads to the reduction of fractional abundances of  $\text{CH}_2\text{CN}$  on the decreased grain surfaces. Thus the abundances of  $\text{CH}_3\text{CN}$  naturally decrease with grain growth (see Figure 8, top).

For the fractional abundances of  $\text{CH}_3\text{OCH}_3$  (see Figure 8, middle), we find that neither the gas-phase nor the grain-surface species are very much affected by grain growth. This is because on ice, the two reactants  $\text{CH}_3$  and  $\text{CH}_2\text{OH}$  do not change their fractional abundances very much with grain growth when  $\text{CH}_3\text{OCH}_3$  is being formed ( $t_{\text{final}} - t \sim 10^5$  years).

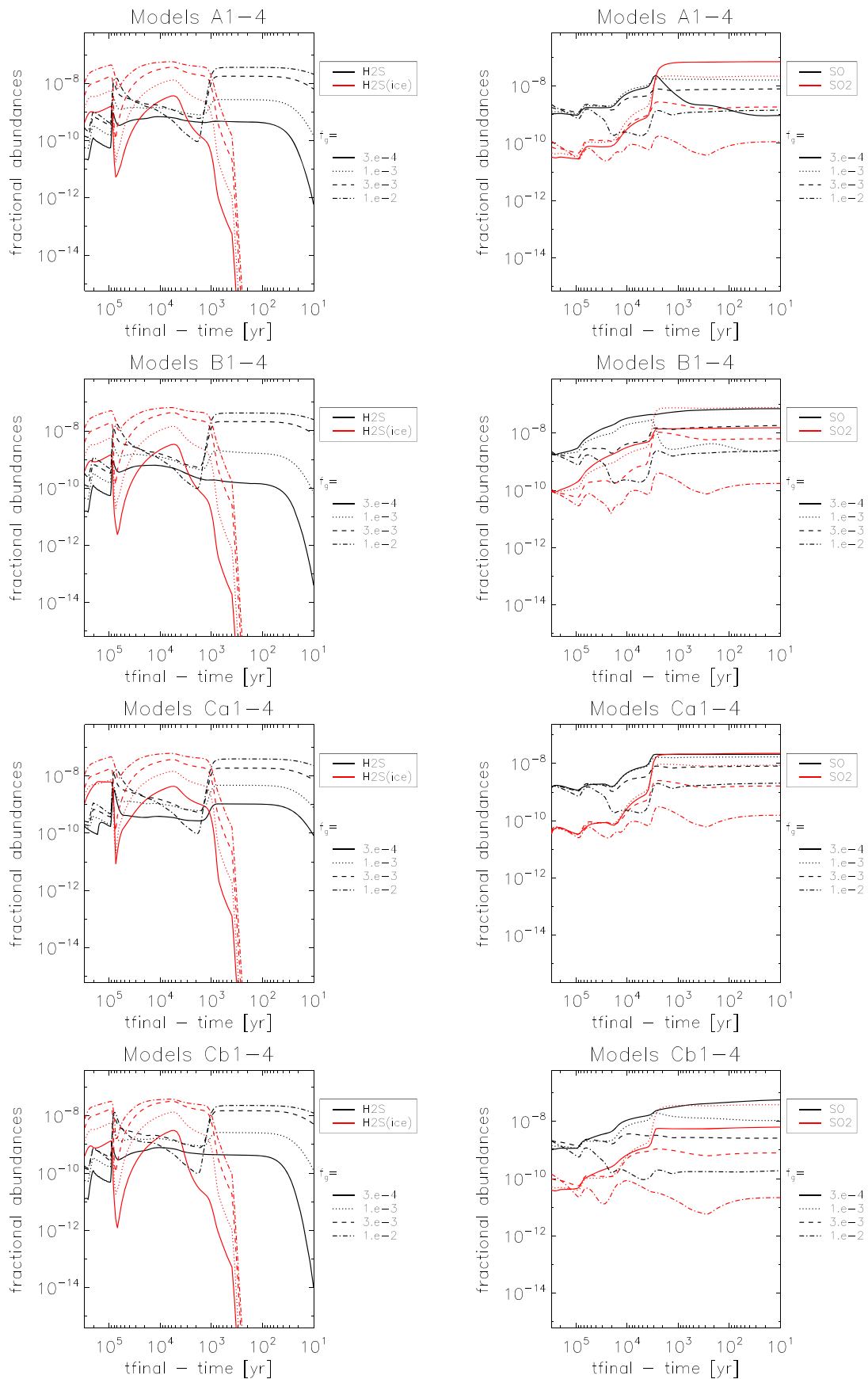
Finally, our results show that fractional abundances of  $\text{HCOOH}$  increase with decreasing values of  $f_g$  (see Figure 8, bottom). It is interesting that the increment is pronounced significantly when  $f_g = 3 \times 10^{-4}$ . We find that this is achieved by the increased fractional abundance of  $\text{O}_2^+$  (see Equation (19)).

### 3.3. Radial Dependence

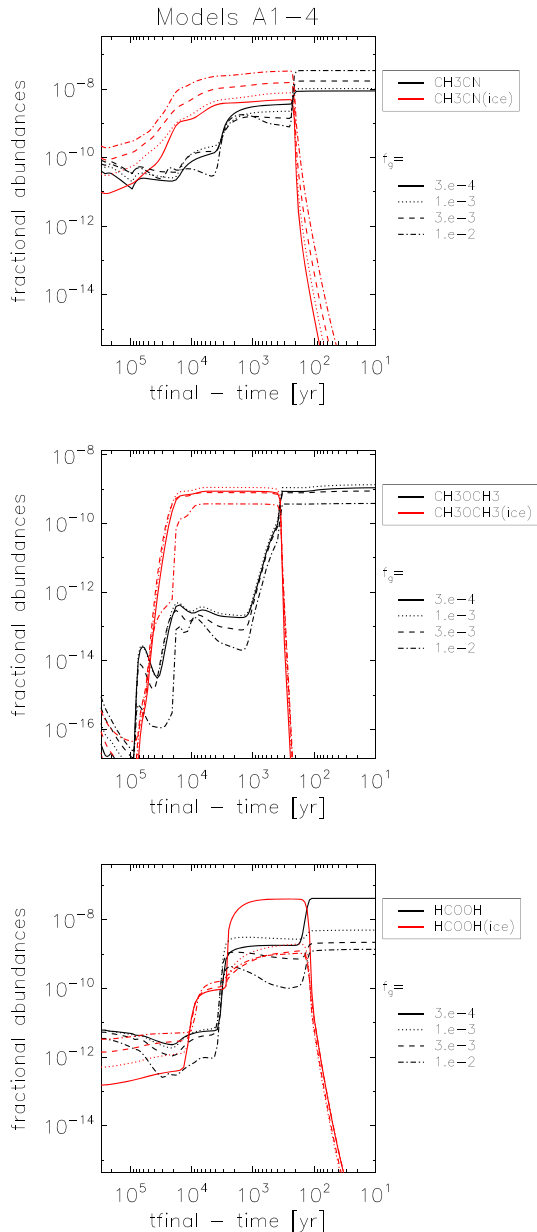
We have so far examined the time evolution of molecules, following an inward-moving shell that eventually arrives at  $r_{\text{final}} = 15$  au. This approach is useful in the sense that we can trace what types of molecules form and how they evolve with time for a certain collapsing gas parcel. At the same time, however, it is valuable to examine molecular evolution as a function of the distance from the central star for a given time. This is because we can then specify the most important location (s) to examine the effect of grain growth on molecular evolution for certain times. Here, we undertake this by computing the resulting fractional abundances of molecules for collapsing shells that finally arrive at  $r = 3\text{--}8000$  au at  $t = t_{\text{final}}$ . We note that we focus on sulfur-bearing molecules and COMs in the following sections. We examine sulfur-bearing molecules because these species can serve as the most direct probe for calibrating the degree of grain growth (see Section 3.2.2, also see below). In addition, we consider the resulting behavior of COMs because their chemistry has been studied as probes of physical conditions of a star-forming cloud, and the effect of grain growth needs to be understood.

Figure 9 (top) shows the fractional abundances of sulfur-bearing molecules for the models without grain growth (Model A1, left panel) and with grain growth (Model A4, right panel), respectively. The resulting molecular distributions are clearly similar to those shown in Figure 2(d) for the model without grain growth and Figure 7 (top left) for the model with grain growth, while the  $x$ -axis should be reversed (that is, small orbital radii correspond to small values of  $t_{\text{final}} - t$ ). This similarity arises from the fact that molecular evolution is determined mainly by the time dependence of the physical conditions (rather than the time evolution of chemistry itself), as we noted in the first part of Section 3. As a result, the radial dependence of the chemistry becomes similar to the time dependence of chemistry for specific values of  $r_{\text{final}}$ . Our results also show that the resulting molecular distributions are quite different between the two cases; for the model without grain growth,  $\text{H}_2\text{S}$  is the dominant molecule in the entire region of the core, except for the innermost radii within 10 au (Figure 9, top left). We note that sublimation of  $\text{H}_2\text{S}$  ice occurs at  $r \simeq 300$  au, where the temperature is about 50 K. In contrast,  $\text{SO}_2$  is dominant at  $r < 500$  au for the model with grain growth (Figure 9, top right). Beyond  $r = 500$  au,  $\text{SO}$  becomes most abundant. This difference originates from grain surface reactions that play an important role in forming  $\text{H}_2\text{S}$ . As discussed in Section 3.2.2, formation of  $\text{H}_2\text{S}$  is suppressed significantly when grain growth is taken into account.

The radial distribution of COMs is shown in Figure 9 (bottom two panels). There is no clear qualitative difference; for both cases,  $\text{CH}_3\text{OH}$  is most abundant in the inner region ( $r < 100$  au) and in the outer region ( $r > 1000$  au), and in the intermediate region  $\text{CH}_3\text{CN}$  is the dominant molecule. Quantitatively, there are noticeable differences (also see Sections 3.1.3 and 3.2.3); at  $r < 100$  au for the model with grain growth, the abundance of  $\text{CH}_3\text{OH}$  is about one order of



**Figure 7.** Fractional abundances of sulfur-bearing molecules as a function of time are shown for an initial condition of (top row)  $A_V^{\text{init}} = 3$  mag and  $t_{\text{qui}} = 10^6$  year, (second row)  $A_V^{\text{init}} = 1$  mag and  $t_{\text{qui}} = 10^6$  year, (third row)  $A_V^{\text{init}} = 3$  mag and  $t_{\text{qui}} = 10^4$  year, and (bottom row)  $A_V^{\text{init}} = 3$  mag and  $t_{\text{qui}} = 10^7$  year. Models with different values of  $f_g$  are shown.



**Figure 8.** Fractional abundances of complex organic species as a function of time are shown for an initial condition of  $A_V^{\text{init}} = 3$  mag and  $t_{\text{quie}} = 10^6$  year. Models with different values of  $f_g$  are shown.

magnitude higher, that of  $\text{CH}_3\text{CN}$  is lower by a factor of about 5, and that of  $\text{HCOOH}$  is more than one order of magnitude higher than for the model without grain growth. It is interesting that  $\text{CH}_3\text{OCH}_3$  has a comparable fractional abundance for the models with and without grain growth.

We can therefore infer the degree of grain growth in the systems under consideration either by spatially resolving the molecular distribution or by measuring the abundance ratios of the above molecules, which we discuss in more detail in the following sections.

#### 4. Discussion

In the above calculations, we have changed the total surface area ( $f_g$ ) of grains and investigated the effect of grain growth on the resulting molecular abundances. In order to directly

compare the results between the models with and without grain growth, we adopted fixed values for the other two parameters ( $A_V^{\text{init}} = 3$  mag and  $t_{\text{quie}} = 10^6$  years) there. Here, we perform a parameter study in which the values of both  $A_V^{\text{init}}$  and  $t_{\text{quie}}$  vary (see Table 4), and explore how molecular evolution is affected by these two parameters for the model with grain growth. In addition, we carry out comparisons with the observations, and examine how grain growth that can potentially occur in the observed systems can be related to the observed molecular abundances. Finally, we discuss other effects that may affect our calculations.

#### 4.1. Dependence on Parameters

We investigate how the fractional abundances of molecules change as a function of both  $A_V^{\text{init}}$  and  $t_{\text{quie}}$  for the grain growth case (see Table 4). Since the degree of grain growth (see Sections 3.2.2 and 3.3) can be best measured on sulfur-bearing molecules, we consider these species ( $\text{H}_2\text{S}$ ,  $\text{SO}$ , and  $\text{SO}_2$ ) in addition to COMs. We show figures only when the resultant fractional abundances change significantly. As in Sections 3.1 and 3.2, a shell that finally arrives at  $r_{\text{final}} = 15$  au is used for chemistry calculations.

##### 4.1.1. The Case of $A_V^{\text{init}} = 1$ mag

We find that when the model with  $A_V^{\text{init}} = 1$  mag (Models B1-4 in Table 4) is considered, initial abundances of stable molecules such as  $\text{CO}$ ,  $\text{H}_2\text{O}$ , and  $\text{NH}_3$  are lower, and more C, O, and N are in ionic or atomic form than in the case of  $A_V^{\text{init}} = 3$  mag. This is simply because the amount of interstellar UV flux received by star-forming clouds increases with decreasing value of  $A_V^{\text{init}}$  (see Section 2.3), and also because the chemistry has not evolved from ionic/atomic form at smaller  $A_V^{\text{init}}$ .

For sulfur-bearing molecules, the  $\text{H}_2\text{S}$  fractional abundances in the case of  $A_V^{\text{init}} = 1$  mag are very similar to those in the case of  $A_V^{\text{init}} = 3$  mag, as shown in Figure 7 (second row). The reason for this is that  $\text{H}_2\text{S}$  is formed via hydrogenation on grain surfaces, which is not directly related to the variation of  $A_V^{\text{init}}$  in our model. In contrast, the fractional abundances of  $\text{SO}$  and  $\text{SO}_2$  depend sensitively on the  $A_V^{\text{init}}$ . Figure 7 (second row) shows their resultant behaviors; we immediately observe that  $\text{SO}$  is more abundant when  $A_V^{\text{init}} = 1$  mag (also see Figure 7 (top) for comparison). This is clearly visible for the case of  $f_g = 3 \times 10^{-4}$ ; there is more free atomic carbon, which can destroy  $\text{SO}_2$  by



The  $\text{SO}/\text{SO}_2$  ratio is also affected by  $\text{OH}$  abundances, and it is prominent for the case of  $f_g = 1 \times 10^{-3}$ . In the gas-phase,  $\text{OH}$  is made from  $\text{O} + \text{H}_2\text{CO} \longrightarrow \text{OH} + \text{HCO}$ , while  $\text{H}_2\text{CO}$  is made via a reaction  $\text{O} + \text{CH}_3 \longrightarrow \text{H}_2\text{CO} + \text{H}$ . When  $f_g$  becomes lower, abundances of atomic oxygen increase, while  $\text{CH}_3$  fractional abundances decrease. For low  $A_V^{\text{init}}$ , the same trend of higher O and lower  $\text{CH}_3$  fractional abundances is observed.  $\text{OH}$  is enhanced when  $A_V^{\text{init}}$  and  $f_g$  have a good balance to produce both O and  $\text{CH}_3$  in moderate abundances.

For COMs, the tendency of lower fractional abundances of  $\text{CH}_3\text{CN}$  with grain growth becomes stronger in the case of  $A_V^{\text{init}} = 1$  mag than in the case of  $A_V^{\text{init}} = 3$  mag; large amounts of  $\text{C}^+$  or O can destroy  $\text{CH}_3\text{CN}$  or its precursors for the former

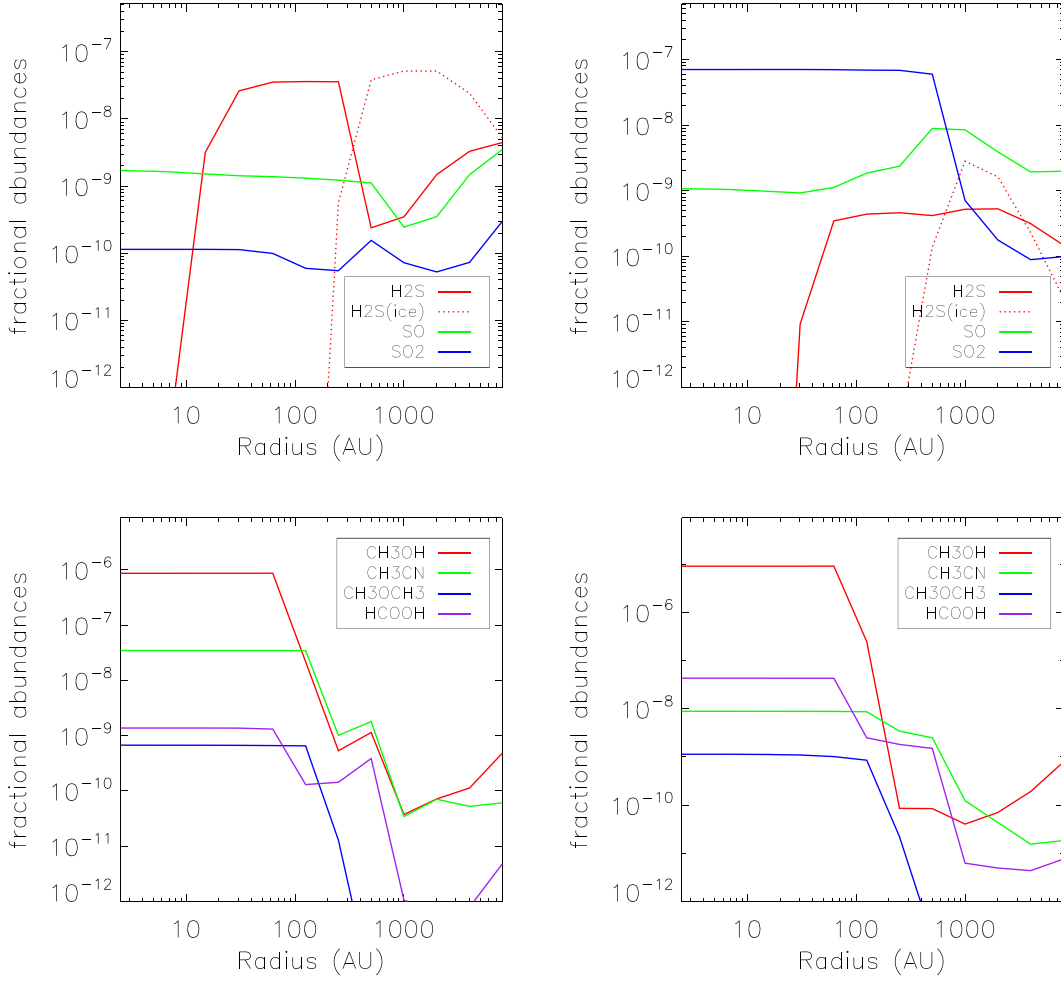


**Figure 9.** Fractional abundances of sulfur-bearing molecules and COMs are shown as a function of radius for (left) the fiducial model (Model A1) and (right) for the grain growth model (Model A4) at  $t = t_{\text{final}}$ .

case. The fractional abundances of  $\text{CH}_3\text{OH}$  and  $\text{CH}_3\text{OCH}_3$  do not change significantly with the change in values of  $A_V^{\text{init}}$ . For  $\text{HCOOH}$ , the difference between  $A_V^{\text{init}} = 1$  mag and 3 mag is less than a factor of a few, except for the case of  $f_g = 1 \times 10^{-3}$ , where the fractional abundance of  $\text{HCOOH}$  is higher by an order of magnitude for  $A_V^{\text{init}} = 1$  mag. This increase is caused by the increased abundance of  $\text{OH}$  in the case of  $f_g = 1 \times 10^{-3}$  and  $A_V^{\text{init}} = 1$  mag, as discussed in the paragraph above.

In brief, the effect of grain growth at  $A_V^{\text{init}} = 1$  mag still causes lower  $\text{H}_2\text{S}$  and higher  $\text{SO}$  or  $\text{SO}_2$ . The difference from the model with  $A_V^{\text{init}} = 3$  mag is that the  $\text{SO}/\text{SO}_2$  ratio increases with grain growth in the model with  $A_V^{\text{init}} = 1$  mag. One noticeable difference for COMs between the models with  $A_V^{\text{init}} = 3$  mag and 1 mag is that  $\text{CH}_3\text{CN}$  fractional abundances decrease more with grain growth when  $A_V^{\text{init}} = 1$  mag.

#### 4.1.2. The Cases of $t_{\text{quie}} = 10^4$ and $10^7$ year

In this section, we present results that are obtained for the cases of  $t_{\text{quie}} = 10^4$  years (Models Ca1-4 in Table 4) and  $10^7$  years (Models Cb1-4 Table 4). Since we change  $f_g$  at the beginning of our calculations, which corresponds to the initial stage of the quiescent phase, a longer  $t_{\text{quie}}$  means that grain growth affects molecular evolution for a longer time.

Therefore, the effect of grain growth should appear more strongly with a longer  $t_{\text{quie}}$ .

Just like in the case of  $A_V^{\text{init}}$ , the fractional abundances of  $\text{H}_2\text{S}$  are not very dependent on  $t_{\text{quie}}$ . But the ratio of  $\text{SO}$  and  $\text{SO}_2$  changes with the variation of  $t_{\text{quie}}$  (Figure 7, third and bottom row). The reason is an increase in the fractional abundance of  $\text{OH}$  around  $t_{\text{final}} - t = 3000$  years in the case of  $t_{\text{quie}} = 10^6$  years, which can help reaction (12), which involves  $\text{OH}$ . As described in Section 4.1.1,  $\text{OH}$  abundances increase when  $f_g$  allows moderate abundances of atomic oxygen and  $\text{CH}_3$ .

For COMs, there is no significant change in the fractional abundances of  $\text{CH}_3\text{OH}$  and  $\text{CH}_3\text{CN}$  with the variation of  $t_{\text{quie}}$ . As shown in Figure 10, fractional abundances of  $\text{CH}_3\text{OCH}_3$  decrease with grain growth when  $t_{\text{quie}} = 10^4$  and  $10^7$  years, unlike the case of  $t_{\text{quie}} = 10^6$  years, where there is no change with grain growth (see Figure 8). This is explained by the abundances of relevant species in reactions (15)–(17). For the cases of  $t_{\text{quie}} = 10^4$  and  $10^7$  years,  $\text{CH}_3$  becomes less abundant with grain growth because hydrogenation is less efficient. The fractional abundances of  $\text{HCOOH}$  increase with grain growth, as discussed in Section 3.2.3. We find that this tendency weakens when  $t_{\text{quie}} = 10^4$  years because the increase in  $\text{O}_2^+$  is less pronounced (Figure 11). There is no obvious change from the models of  $t_{\text{quie}} = 10^6$  years when  $t_{\text{quie}} = 10^7$  years.

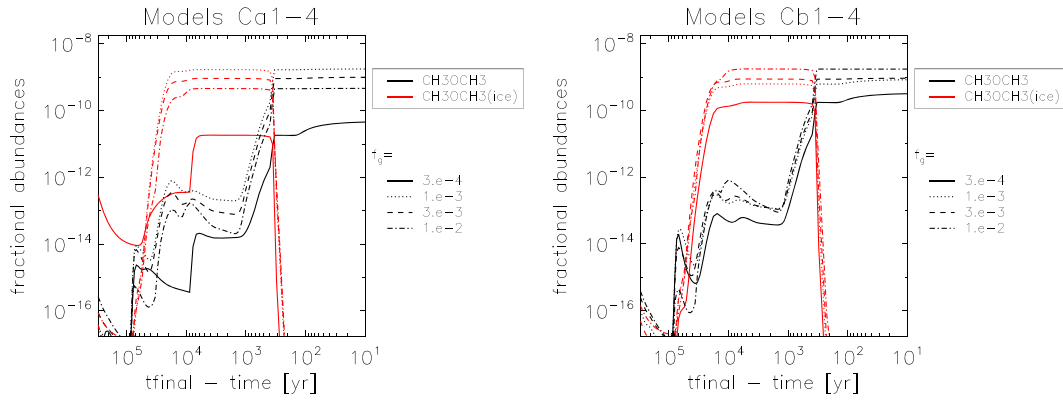


**Figure 10.** Similar to Figure 8 (middle), but for  $t_{\text{qui}} = 10^4$  year (top) and  $t_{\text{qui}} = 10^7$  year (bottom).

In summary, the parameter  $t_{\text{quie}}$  can influence some of sulfur-bearing molecules (SO and  $\text{SO}_2$ ) that are important for inferring the degree of grain growth for observed YSOs. Qualitatively, however, our conclusion is unchanged; SO and  $\text{SO}_2$  become more abundant than  $\text{H}_2\text{S}$  if  $f_g \lesssim 3 \times 10^{-3}$ .

#### 4.2. Change of $A_V$ with Grain Growth

As mentioned in Section 2.1, the dependence of  $A_V$  on dust properties can also affect the chemistry. In this section, we discuss the effect of  $A_V$  when they are scaled with  $f_g$  (Models D1-4). We focus on a moving shell that arrives at  $r_{\text{final}} = 15$  au. To proceed, we use the following method for our chemistry calculations. The values of  $A_V$  should scale as  $a_{\text{max}}^{-1/2} \propto f_g$  (see Figure 1 in Aikawa & Nomura 2006). Accordingly, we can use a formula that is written as  $A_V = N_{\text{H}}(f_g/0.01)/(1.59 \times 10^{21} \text{ cm}^2)$  (i.e., smaller  $A_V$  with grain growth). We still assume that a core is embedded, and  $A_V$  of 3 mag is added to this derived  $A_V$ .

In these models, we find that the main effect of grain growth on the sulfur-bearing molecules is relatively unchanged. As shown in Figure 13, fractional abundances of  $\text{H}_2\text{S}$  decrease with grain growth, and the dominant form of sulfur is taken over by SO and  $\text{SO}_2$ . The main difference in Models D2-4 from the Models A2-4 are higher abundance ratios of SO over  $\text{SO}_2$ . This difference comes from the effect of lower visual extinction. As shown in Figure 12,  $A_V$  stays below 4 mag until  $t_{\text{final}} - t = 100$  years in Model D4. At this low  $A_V$ , direct photodissociation efficiently converts  $\text{SO}_2$  into SO. Despite this difference, ratios between  $\text{H}_2\text{S}$ , SO, and  $\text{SO}_2$  can still act as useful diagnostics for grain growth.

On the other hand, fractional abundances of COMs are greatly affected by the decreased  $A_V$  with grain growth. Fractional abundances of  $\text{CH}_3\text{OH}$  in Model D4 are more than an order of magnitude lower than those for the case of Models D1-2 in the gas phase and on grains because of photodissociation (Figure 13; bottom left). This trend of lower fractional abundances with lower  $f_g$  also applies to  $\text{CH}_3\text{OCH}_3$  (Figure 13; bottom right) and other COMs as a result of efficient photodissociation.

Although  $A_V$  should indeed scale with  $f_g$  as in this section theoretically, it is unlikely that the actual values of  $A_V$  are orders of magnitude lower than the valued adopted for the ISM case. The reason is that infrared observations of cold dark clouds have shown moderate values of  $A_V$  ( $>10$ ) at a large radius  $R < 7000$  au (Alves et al. 2001). It is therefore more likely that star-forming clouds are shielded from UV photos,

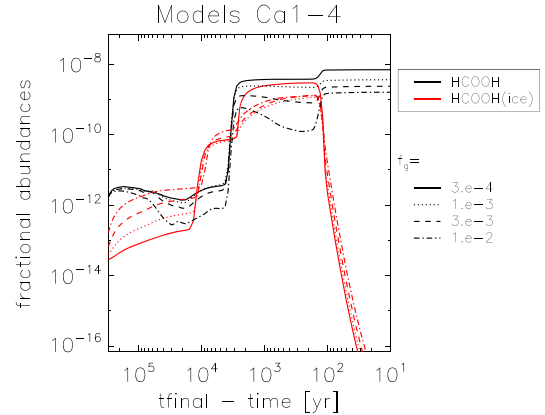


**Figure 11.** Similar to Figure 8 (bottom), but for  $t_{\text{qui}} = 10^4$  year.

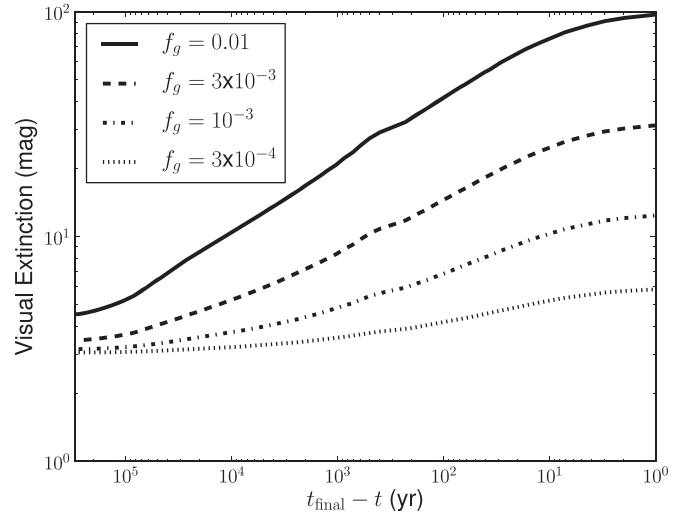


**Figure 12.** Values of visual extinction as functions of time in Models D1-4 at  $r_{\text{final}} = 15$  au.

and hence our chemistry calculations performed in other sections may better represent the observed clouds.

#### 4.3. Comparisons with Molecular Observations

Keeping in mind the above sensitivity of our results to model parameters, we here compare our results with interferometric observations of protostellar systems. This is undertaken to obtain some insights about how the effect of grain growth can

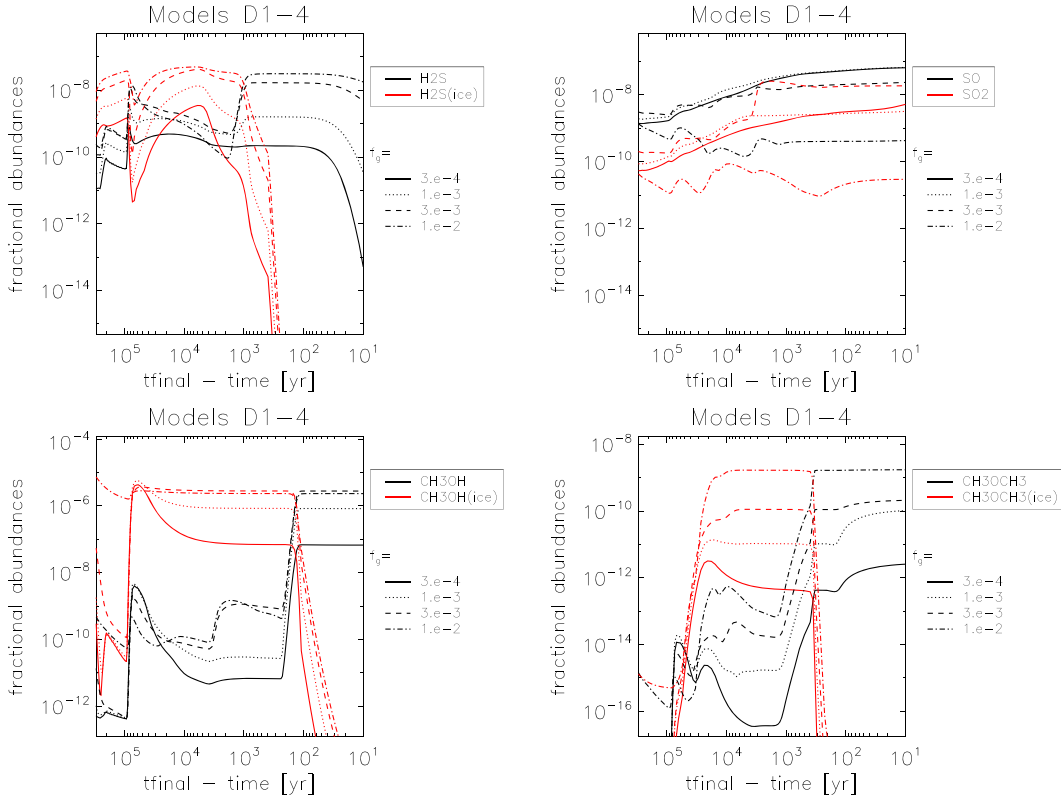


**Figure 13.** Fractional abundances of (top) sulfur-bearing molecules and (bottom) selected COMs for  $A_V^{\text{init}} = 3$  mag and  $t_{\text{quie}} = 10^6$  years, while values of  $A_V$  are scaled with  $f_g$ .

be perceived in the observed molecular abundances. As examples, we consider IRAS 16293-2422 (hereafter IRAS 16293) and NGC 1333-IRAS 2A (hereafter IRAS 2A).

IRAS 16293 is a well-studied class 0 protostellar system ( $d = 120$  pc; Loinard et al. 2007) in  $\rho$  Ophiuchus. For this target, a number of molecular species have been detected so far (e.g., Schöier et al. 2002; Kuan et al. 2004; Chandler et al. 2005; Bisschop et al. 2008; Caux et al. 2011; Jørgensen et al. 2011). It is also reported that the target contains two components, A and B, and component A can be separated into even more complex structures. Furthermore, an outflow has been found in component A (Walker et al. 1988; Yeh et al. 2008; Girart et al. 2014), and an association of each part of component A with the outflow has been proposed (e.g., Loinard et al. 2007). IRAS 2A, which is located in NGC 1333 ( $d = 235$  pc, Hirota et al. 2008), is classified as a class 0 protostar, and an outflow has been observed. There are other hot cores in NGC 1333, such as NGC 1333-IRAS 4A and NGC 1333-IRAS4B, and their chemistry has been studied by many authors (Blake et al. 1995; Bottinelli et al. 2007). We nonetheless choose IRAS 2A because its fractional abundances of COMs are higher than those in NGC 1333-IRAS 4A, and an interferometric observation of COMs by Taquet et al. (2015) is available.

While the complexity observed in these sources cannot be easily included in our current model, we compare the overall observed chemical abundances with our results. In order to proceed, we make use of the following observational data: for IRAS 16293, Chandler et al. (2005) detected some sulfur-bearing molecules using the submillimeter array with high ( $1''$ – $2''$ ) angular resolution, and for IRAS 2A, Taquet et al. (2015) derived the chemical abundances using the Plateau de Bure

interferometer with the  $\sim 2''$  beam, assuming a source size of  $0''.5$ .

We derive the average fractional abundances of species  $X_i$  within the beam in our model by calculating

$$\langle X_i \rangle = \frac{\int_0^{R_{\text{max}}} 2\pi R N(R, i) dR}{\int_0^{R_{\text{max}}} 2\pi R N_{\text{Htot}}(R) dR}, \quad (22)$$

where  $R$  is a distance from the center on a plane perpendicular to the line of sight,  $N(R, i)$  is the column density of species  $i$  along the line of sight at  $R$ , and  $N_{\text{Htot}}(R)$  is the total hydrogen column density along  $R$ . We use  $R_{\text{max}} = 120$  au for IRAS 16293 ( $\sim 2''$ -diameter around the beam size), and  $R_{\text{max}} = 60$  au for IRAS 2A ( $\sim 0''.5$  diameter; the source size). In the following, we compare our results with the observed values and attempt to derive the degree of grain growth for the targets.

#### 4.3.1. Sulfur-bearing Molecules

As discussed in Section 3.2.2, the resulting abundances of SO, SO<sub>2</sub>, and H<sub>2</sub>S can serve as a good tracer of grain growth. Here we compute the SO<sub>2</sub>/SO and H<sub>2</sub>S/SO ratios, and obtain a possible value of  $f_g$  that can reproduce the observations of IRAS 16293 reported by Chandler et al. (2005). It should be noted that we here use sulfur elemental abundances that are an order of magnitude higher than the fiducial case. This enhancement is required to obtain a better fit to the observed fractional abundances.

Figure 14 shows the results of these ratios. In this plot, the observed values are also included, wherein the volume-averaged fractional abundances of the observed molecules are

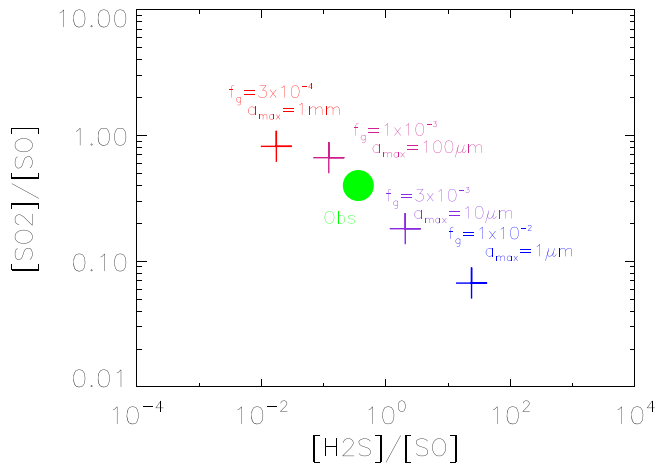


**Figure 14.** Abundance ratios of  $\text{H}_2\text{S}/\text{SO}$  and  $\text{SO}_2/\text{SO}$  are shown for  $A_V^{\text{init}} = 3$  mag,  $t_{\text{quie}} = 10^6$  years, with varying ratios of the dust to gas mass of  $f_g = 3 \times 10^{-4} - 1 \times 10^{-2}$  with blue, blue-violet, violet-red, and red crosses. The observed value by Chandler et al. (2005) is also shown as a green circle.

computed under the assumption that the fractional abundances of these species are uniform within the emitting areas. Since sources A and B are both averaged, we only have one value of fractional abundance per molecule. We find that models with  $f_g = 1 \times 10^{-3} - 3 \times 10^{-3}$  are in good agreement with the observed ratios of sulfur-bearing molecules. It is important that these two cases correspond to grain growth by factors of 10–100, i.e.,  $a_{\text{max}} = 10 - 100 \mu\text{m}$ . Even when other values of  $A_V^{\text{init}}$  and  $t_{\text{quie}}$  are used, the observed values show good agreement with this range. Furthermore, we have confirmed that this trend is not affected by the enhancement of sulfur abundances. This is simply because the resulting abundance ratio of sulfur containing species is not changed by this enhancement. The only exception is  $f_g = 3 \times 10^{-4}$ , where the  $\text{SO}_2/\text{SO}$  ratio decreases by about 2 orders of magnitude for the fiducial case. This is the outcome of the lack of available elemental oxygen to keep a high enough abundance of  $\text{SO}_2$  in this particular case. Our comparison thus suggests that it may be possible to infer the degree of grain growth by observing sulfur-bearing molecules.

#### 4.3.2. COMs

For COMs, the situation is less promising. This occurs because it becomes more difficult to reproduce the observed values within the parameter space we consider. This disagreement between the observation and models already existed in Aikawa et al. (2008).

As in the above section, we compute the volume-averaged fractional abundances of some COMs at  $t = t_{\text{final}}$ , assuming that the physical size of IRAS 2A is  $r_{\text{max}} = 60$  au. For the observed values, the rotational diagram analysis is used with the assumption of a source size of 0.5 (Taquet et al. 2015).

Table 5 summarizes the resulting values. It is obvious that our fractional abundances of  $\text{CH}_3\text{OH}$  in the gas-phase are overproduced in all of models. The difference with the observed values becomes larger when grain growth proceeds further. For  $\text{CH}_3\text{CN}$ , the fractional abundances are again overproduced in our models. However, we find that the deviation with the observations becomes less significant when the effect of grain growth is considered. Finally, the results show that our fractional abundances of  $\text{CH}_3\text{OCH}_3$

underproduce the observed values by at least a factor of several. Even when other values of  $A_V^{\text{init}}$ ,  $t_{\text{quie}}$  are used, this disagreement does not disappear. This shows that it is difficult to reproduce the observed abundance of COMs by tuning the parameters we consider in this paper ( $f_g$ ,  $A_V^{\text{init}}$ ,  $t_{\text{quie}}$ ).

#### 4.4. Other Related Factors

We have found in the last section that sulfur-bearing molecules can act as a good calibrator of grain growth, but it is very difficult to use the abundance of COMs for the purpose. We here discuss why this difference occurs, especially focusing on our assumptions.

First, the reaction routes of COMs may need to be revisited. Taquet et al. (2016) recently studied the formation of COMs through evaporation of methanol and ethanol followed by gas-phase ion-neutral reactions. Inclusion of proton-transfer reactions with ammonia is also a key for the formation of larger COMs such as  $\text{CH}_3\text{OCH}_3$ ,  $\text{CH}_3\text{OCHO}$ , and  $\text{C}_2\text{H}_5\text{OCH}_3$  because some protonated COMs such as  $\text{CH}_3\text{OH}_2^+$  and  $\text{C}_2\text{H}_5\text{OH}_2^+$  help form larger COMs. The rates of these gas-phase reactions as well as surface reactions need to be explored in detail.

In addition, we assume a spherically symmetric 1D envelope structure here. A multidimensional structure such as used in Drozdovskaya et al. (2016) may also play a role, although their model produces COMs in the very vicinity of the protostar in the gas-phase ( $r < 50$  au). this consideration is beyond the scope of this paper.

We may also wonder how properties of dust particles such as porosity would affect our results. In this study, we have assumed that dust grains are compact and spherical to be able to include the effect of grain growth (see Section 2.4). It has been suggested, however, that the porosity of dusty aggregates may be important for the growth and the transport of dusty aggregates (e.g., Ormel et al. 2007; Blum & Wurm 2008; Okuzumi et al. 2012). We can readily examine this effect by considering how the total surface area of dusty aggregates changes, depending on the porosity. Based on the recent studies, the fractal dimension ( $d_f$ ) of dusty aggregates in protoplanetary disks may be given as  $d_f \approx 2$  (e.g., Okuzumi et al. 2009). If this were also the case for protostellar envelopes, the bulk density ( $\rho_{\text{gr}}$ ) of dusty aggregates would become  $\rho_{\text{gr}} \propto a^{-1}$ . In this case, the total surface area becomes independent of the aggregate size. As discussed above, some degree of the reduction in the total surface areas would be needed to reproduce the observed abundance ratio of sulfur-bearing molecules (see Figure 14). Furthermore, our results indicate that the model without grain growth also has difficulties in fitting the observed abundances of COMs. The dust properties are therefore unlikely to be one of the main reasons for the difference between our results and the observed ones, especially for COMs.

## 5. Summary

Dust growth is one of the fundamental processes that can occur in the stage of both star and planet formation. Recent radio interferometric observations boost its importance; these observations imply that a number of class 0–I YSOs might possess millimeter-sized dust grains. While the ultimate origin of these grains is still unknown, it would be readily anticipated that the presence of such grains can affect the chemical

**Table 5**  
Observed and Modeled Fractional Abundances of COMs

Species	Observed	Modeled Fractional Abundances			
		$f_g = 1 \times 10^{-2}$	$3 \times 10^{-3}$	$1 \times 10^{-3}$	$3 \times 10^{-4}$
CH <sub>3</sub> OH	$(2.5 \pm 0.9) \times 10^{-7}$	4.7(−7)	2.5(−6)	5.3(−6)	4.9(−6)
CH <sub>3</sub> CN	$(2.0 \pm 0.4) \times 10^{-9}$	2.4(−8)	1.2(−8)	7.4(−9)	6.5(−9)
CH <sub>3</sub> OCH <sub>3</sub>	$(8.2 \pm 3.3) \times 10^{-9}$	4.5(−10)	6.1(−10)	8.7(−10)	6.9(−10)
HCOOH	...	7.9(−10)	1.4(−9)	3.6(−9)	2.4(−8)

**Note.** Modeled fractional abundances are for  $A_V^{\text{init}} = 3$  mag and  $t_{\text{quie}} = 10^6$  years. The notation  $a(-b)$  indicates  $a \times 10^{-b}$ .

compositions of the systems, and hence provide an invaluable opportunity to obtain additional constraints on the formation of stars and planets.

In this paper, we made use of a gas-grain chemical model, coupled with a physical model of a star-forming cloud in a post-processing fashion. We performed a comprehensive analysis of the influence of grain growth on the molecular evolution of the cloud. This has been achieved by our parameterized approach of grain growth, following the degree of grain growth (see Equation (6)). In addition, we have undertaken a parameter study by changing other model parameters such as the time interval ( $t_{\text{quie}}$ ) of a quiescent phase before a star-forming cloud collapses, and the visual extinction ( $A_V^{\text{init}}$ ) of a cloud that can regulate the initial molecular abundances (see Table 3).

One of the most important findings in this paper is that sulfur-bearing molecules such as H<sub>2</sub>S, SO, and SO<sub>2</sub> can be used as probes of grain growth. This is possible because the change in the fractional abundance of sulfur-bearing molecules is quite intuitive (see Figure 7): when grain growth is included, the abundance of H<sub>2</sub>S decreases since hydrogenation on grain surfaces is the main route to form it. This reduction in turn forms SO and SO<sub>2</sub> more abundantly. We can therefore calibrate the degree of grain growth by computing the abundance ratios among them. Another possibility to quantify the degree of grain growth is the spatial distribution of sulfur-bearing molecules (see Figure 9 (top)). Our results show that while H<sub>2</sub>S is prevalent across the entire region of a star-forming cloud for the case of no grain growth, SO<sub>2</sub> becomes the most abundant, especially in the inner region ( $r \lesssim 1000$  au) of the cloud, when grain growth is included. This shows that sulfur-bearing molecules are most useful to identify how significant grain growth is in the systems under consideration.

Our results also show that inclusion of grain growth generates a variety of changes in the fractional abundances of molecules. There is a significant change in the fractional abundance for the dominant form of carbon-bearing species. Our results show that the abundance of CO in the gas phase increases considerably as a result of the effect of grain growth (see Figure 4). For COMs, the situation is more complicated: as grain growth proceeds, the fractional abundance of CH<sub>3</sub>CN decreases, the fractional abundance of CH<sub>3</sub>OCH<sub>3</sub> does not change very much, and the fractional abundance of HCOOH increases (see Figure 8). This complexity arises because these molecules are the outcome of a number of chemical reactions and their reactants, which also experience various changes due to grain growth.

We have performed a parameter study about other model parameters (see Table 4). We find that the variation of  $A_V^{\text{init}}$  and  $t_{\text{quie}}$  does not affect the trend of the fractional abundance of

H<sub>2</sub>S; its abundance decreases with the degree of grain growth. Conversely, the ratio of SO/SO<sub>2</sub> can be altered by values of  $A_V^{\text{init}}$  and  $t_{\text{quie}}$ . This implies that some care is needed to quantify the degree of grain growth by using the abundance ratios of sulfur-bearing molecules. For COMs, the resulting behaviors are again complex. As an example, we find that the resulting changes of the fractional abundance for CH<sub>3</sub>CN and HCOOH are qualitatively consistent for a wide range of  $A_V^{\text{init}}$  or  $t_{\text{quie}}$ ; the former becomes less abundant with grain growth, while the latter becomes richer for the case of grain growth. Our results show, however, that the resulting decrement or increment of these two COMs is quantitatively different for different values of  $A_V^{\text{init}}$  or  $t_{\text{quie}}$ . For CH<sub>3</sub>OCH<sub>3</sub>, the increase or decrease in its fractional abundance with grain growth is a function of either  $A_V^{\text{init}}$  or  $t_{\text{quie}}$ . The abundance of COMs may therefore not be a good tracer of grain growth, because their abundances tend to be affected both by grain growth and by other parameters ( $A_V^{\text{init}}$  or  $t_{\text{quie}}$ ).

We have conducted comparisons with the currently existing observations. The observational data taken toward the class 0 protostar IRAS 16293-2422 were used. We attempted to determine the significance of grain growth in the target by focusing on sulfur-bearing molecules (H<sub>2</sub>S, SO, and SO<sub>2</sub>). Our results show that the observational data can be reproduced well when grain growth proceeds by a factor of 10–100, which indicates  $a_{\text{max}} = 10\text{--}100 \mu\text{m}$ . We also carried out a similar comparison for COMs. For this case, the data obtained from NGC 1333-IRAS 2A were used. In contrast to the case of sulfur-bearing molecules, we found that our model cannot reproduce the observed values by only adjusting the degree of grain growth within the range of parameters we consider. We discussed potential reasons for our failure to determine a good set of parameters for COMs. While the main reason is not entirely obvious, formation reactions of COMs need to be explored further.

ALMA observations have recently become available with significantly higher sensitivities and angular resolutions. These observations and chemical modeling in this paper would be central to understand when and to which degree grain growth occurs during the course of star formation, and how the resulting molecular evolution is affected by the presence of larger grains.

We are grateful to the anonymous referee for the insightful comments, and to Kenji Furuya for providing data of his cloud formation model. Part of this research was carried out at JPL/Caltech, under a contract with NASA. Y.H. is supported by JPL/Caltech. H.H. is supported by the Ministry of Science and Technology grant MOST 105-2112-M-001-027-MY3, and N. Hirano is supported by MOST 105-2112-M-011-026.

## References

- Acharyya, K., Hassel, G. E., & Herbst, E. 2011, *ApJ*, 732, 73
- Aikawa, Y. 2013, *ChRv*, 113, 8961
- Aikawa, Y., & Herbst, E. 1999, *ApJ*, 526, 314
- Aikawa, Y., & Nomura, H. 2006, *ApJ*, 642, 1152
- Aikawa, Y., Wakelam, V., Garrod, R. T., & Herbst, E. 2008, *ApJ*, 674, 984
- Alves, J. F., Lada, C. J., & Lada, E. A. 2001, *Natur*, 409, 159
- Benz, W., Ida, S., Alibert, Y., Lin, D., & Mordasini, C. 2014, in *Protostars and Planets VI*, ed. H. Beuther et al. (Tucson, AZ: Univ. of Arizona Press), 691
- Bergin, E. A., Hartmann, L. W., Raymond, J. C., & Ballesteros-Paredes, J. 2004, *ApJ*, 612, 921
- Birnstiel, T., Dullemond, C. P., & Brauer, F. 2009, *A&A*, 503, L5
- Bisschop, S. E., Jørgensen, J. K., Bourke, T. L., Bottinelli, S., & van Dishoeck, E. F. 2008, *A&A*, 488, 959
- Blake, G. A., Sandell, G., van Dishoeck, E. F., et al. 1995, *ApJ*, 441, 689
- Blum, J., & Wurm, G. 2008, *ARA&A*, 46, 21
- Bottinelli, S., Ceccarelli, C., Williams, J. P., & Lefloch, B. 2007, *A&A*, 463, 601
- Caselli, P., Hasegawa, T. I., & Herbst, E. 1998, *ApJ*, 495, 309
- Caux, E., Kahane, C., Castets, A., et al. 2011, *A&A*, 532, A23
- Chandler, C. J., Brogan, C. L., Shirley, Y. L., & Loinard, L. 2005, *ApJ*, 632, 371
- Chiang, H.-F., Looney, L. W., & Tobin, J. J. 2012, *ApJ*, 756, 168
- Doty, S. D., Schöier, F. L., & van Dishoeck, E. F. 2004, *A&A*, 418, 1021
- Drozdovskaya, M. N., Walsh, C., van Dishoeck, E. F., et al. 2016, *MNRAS*, 462, 977
- Dullemond, C. P., & Dominik, C. 2005, *A&A*, 434, 971
- Dutrey, A., Semenov, D., Chapillon, E., et al. 2014, in *Protostars and Planets VI*, ed. H. Beuther et al. (Tucson, AZ: Univ. of Arizona Press), 317
- Forbrich, J., Lada, C. J., Lombardi, M., Román-Zúñiga, C., & Alves, J. 2015, *A&A*, 580, A114
- Furuya, K., Aikawa, Y., Hincelin, U., et al. 2015, arXiv:1510.05135
- Garrod, R. T., Wakelam, V., & Herbst, E. 2007, *A&A*, 467, 1103
- Girart, J. M., Estalella, R., Palau, A., Torrelles, J. M., & Rao, R. 2014, *ApJL*, 780, L11
- Hasegawa, T. I., & Herbst, E. 1993, *MNRAS*, 261, 83
- Herbst, E., & Cuppen, H. M. 2006, *PNAS*, 103, 12257
- Herbst, E., & van Dishoeck, E. F. 2009, *ARA&A*, 47, 427
- Hersant, F., Wakelam, V., Dutrey, A., Guilloteau, S., & Herbst, E. 2009, *A&A*, 493, L49
- Hirashita, H., & Li, Z.-Y. 2013, *MNRAS*, 434, L70
- Hirota, T., Bushimata, T., Choi, Y. K., et al. 2008, *PASJ*, 60, 37
- Johansen, A., Mac Low, M.-M., Lacerda, P., & Bizzarro, M. 2015, *SciA*, 1, 1500109
- Jørgensen, J. K., Bourke, T. L., Myers, P. C., et al. 2007, *ApJ*, 659, 479
- Jørgensen, J. K., Bourke, T. L., Nguyen Luong, Q., & Takakuwa, S. 2011, *A&A*, 534, A100
- Jørgensen, J. K., van der Wiel, M. H. D., Coutens, A., et al. 2016, arXiv:1607.08733
- Kataoka, A., Okuzumi, S., Tanaka, H., & Nomura, H. 2014, *A&A*, 568, A42
- Kruegel, E. (ed.) 2003, *The Physics of Interstellar Dust* (Bristol: Institute of Physics Publishing)
- Kuan, Y.-J., Huang, H.-C., Charnley, S. B., et al. 2004, *ApJL*, 616, L27
- Kwon, W., Looney, L. W., Mundy, L. G., Chiang, H.-F., & Kemball, A. J. 2009, *ApJ*, 696, 841
- Li, J. I. H., Liu, H. B., Hasegawa, Y., & Hirano, N. 2017, *ApJ*, submitted
- Li, Z.-Y., Banerjee, R., Pudritz, R. E., et al. 2014, in *Protostars and Planets VI*, ed. H. Beuther et al. (Tucson, AZ: Univ. of Arizona Press), 173
- Linsky, J. L. 2003, *SSRv*, 106, 49
- Loinard, L., Torres, R. M., Mioduszewski, A. J., et al. 2007, *ApJ*, 671, 546
- Masunaga, H., & Inutsuka, S.-i. 2000, *ApJ*, 531, 350
- Mathis, J. S., Rumpl, W., & Nordsieck, K. H. 1977, *ApJ*, 217, 425
- Miotello, A., Testi, L., Lodato, G., et al. 2014, *A&A*, 567, A32
- Natta, A., Testi, L., Calvet, N., et al. 2007, in *Protostars and Planets V*, ed. B. Reipurth et al. (Tucson, AZ: Univ. of Arizona Press), 767
- Öberg, K. I., Fuchs, G. W., Awad, Z., et al. 2007, *ApJL*, 662, L23
- Okuzumi, S., Tanaka, H., Kobayashi, H., & Wada, K. 2012, *ApJ*, 752, 106
- Okuzumi, S., Tanaka, H., & Sakagami, M.-a. 2009, *ApJ*, 707, 1247
- Ormel, C. W., Paszun, D., Dominik, C., & Tielens, A. G. G. M. 2009, *A&A*, 502, 845
- Ormel, C. W., Spaans, M., & Tielens, A. G. G. M. 2007, *A&A*, 461, 215
- Pauly, T., & Garrod, R. T. 2016, *ApJ*, 817, 146
- Ricci, L., Testi, L., Natta, A., & Brooks, K. J. 2010, *A&A*, 521, A66
- Sakai, N., & Yamamoto, S. 2013, *ChRv*, 113, 8981
- Schöier, F. L., Jørgensen, J. K., van Dishoeck, E. F., & Blake, G. A. 2002, *A&A*, 390, 1001
- Semenov, D., Hersant, F., Wakelam, V., et al. 2010, *A&A*, 522, A42
- Taquet, V., López-Sepulcre, A., Ceccarelli, C., et al. 2015, *ApJ*, 804, 81
- Taquet, V., Wirström, E. S., & Charnley, S. B. 2016, *ApJ*, 821, 46
- Testi, L., Birnstiel, T., Ricci, L., et al. 2014, in *Protostars and Planets VI*, ed. H. Beuther et al. (Tucson, AZ: Univ. of Arizona Press), 339
- Tobin, J. J., Hartmann, L., Chiang, H.-F., et al. 2013, *ApJ*, 771, 48
- van Dishoeck, E. F., Bergin, E. A., Lis, D. C., & Lunine, J. I. 2014, in *Protostars and Planets VI*, ed. H. Beuther et al. (Tucson, AZ: Univ. of Arizona Press), 835
- van Dishoeck, E. F., & Blake, G. A. 1998, *ARA&A*, 36, 317
- Walker, C. K., Lada, C. J., Young, E. T., & Margulis, M. 1988, *ApJ*, 332, 335
- Wong, Y. H. V., Hirashita, H., & Li, Z.-Y. 2016, *PASJ*, 68, 67
- Yeh, S. C. C., Hirano, N., Bourke, T. L., et al. 2008, *ApJ*, 675, 454
- Zhao, B., Caselli, P., Li, Z.-Y., et al. 2016, *MNRAS*, 460, 2050